NASA CR-54410
TMC REPORT 25,168

N65-34229	
(ACCESSION NUMBER)	(THRU)
74	1
(PAGES)	(CODE)
CR-54410	28
(NASA CR OR TMX OR AD NUMBER)	(CATEGORY)

FACILITY FORM 602

THE DESIGN AND PERFORMANCE OF A 3KW CONCENTRIC TUBE RESISTOJET

by

R. J. Page and R. A. Short

prepared for

NATIONAL AERONAUTICS AND SPACE ADMINISTRATION

Contract NASW-1070

GPO PRICE $ ______

CFSTI PRICE(S) $ ______

Hard copy (HC) $3.00

Microfiche (MF) 75¢

ff 653 July 65

THE MARQUARDT CORPORATION

Requests for copies of this report should be referred to:

National Aeronautics and Space Administration
Office of Scientific and Technical Information
Attention: AFSS-A
Washington, D.C. 20546

NASA CR-54410
TMC Report 25,168

FINAL REPORT

THE DESIGN AND PERFORMANCE OF A 3 KW CONCENTRIC TUBE RESISTOJET

by

R. J. Page and R. A. Short

prepared for

NATIONAL AERONAUTICS AND SPACE ADMINISTRATION

September 1965

CONTRACT NASW-1070
Technical Management,
NASA, Lewis Research Center
Cleveland, Ohio
Electrothermal Technology Section
Henry R. Hunczak

THE MARQUARDT CORPORATION
16555 Saticoy Street
Van Nuys, California

CONTENTS

Figures

Tables

SYMBOLS

A_e	nozzle exhaust area, cm^2
C_D	discharge coefficient
E	electrode voltage, volts
F	thrust, grams-force
g°	980.665 cm/sec^2
h_i	initial gas enthalpy, cal/gm
I	current, amp
I_{sp}	specific impulse, sec
$\dot{m}$	propellant mass flow, gm/sec
p_{cell}	test cell pressure, grams-force/cm^2
P_e	electric power, watts
P_{g_i}	initial propellant power, watts
P_t	total power, watts
PR_N	pressure ratio across nozzle
η_o	overall total power efficiency (see Appendix B)
η_o^*	overall electric power "efficiency"(see Appendix B)
η_N	nozzle efficiency
η_H	heat exchanger efficiency
η_F	frozen flow efficiency
η_E	expansion efficiency
η_D	divergence efficiency
η_T	thermal efficiency
η_V	viscous efficiency
ρ_a	density of air
ρ_h	density of hydrogen gas

THE DESIGN AND PERFORMANCE OF A 3 KW CONCENTRIC TUBE RESISTOJET

by R. J. Page and R. A. Short

The Marquardt Corporation

I. SUMMARY

Results are reported on the design, fabrication and testing of a 3 kw concentric tube Resistojet using hydrogen as a propellant. The basis of this design was that of an earlier 30 kw unit successfully tested for the Air Force.

Performance during a 25-hour test was an observed specific impulse of 828 seconds and a measured thrust of 65.7 grams force for 3.04 kw of electric power input. The overall efficiency, which includes the input power of the gas was 77 percent. The thrust stagnation conditions were a pressure of 8.8 atmospheres and a gas temperature of 2417 degrees Kelvin.

The heat exchanger (4 cm diameter x 14 cm long overall) consists of eleven cylindrical, tungsten elements of ~ 0.01 mm, or greater, wall thickness. The central nine of these are connected in series and electrically heated.

A tungsten vapor deposition process was used which permitted element shapes of the desired special geometries. This made possible a single boron-nitride insulator or element support which was located in a relatively cool site favoring a long service life.

The heat exchanger efficiency, η_H, that is, the fraction of the total power which is delivered in the hydrogen propellant to the nozzle entrance, was measured to be ~ 0.90. The nozzle energy efficiency, η_N was ~ 0.86 where the geometrical area ratio was 191. Viscous losses in the nozzle, operating at a throat Reynolds number of 3750, based on a diameter of 0.747 mm, were found to be small.

The engine that was performance-tested at Marquardt has been delivered to the Lewis Research Center, NASA, for endurance testing.

Perhaps the most important feature of the concentric tube design is that the maximum temperature of the heating element is only slightly above the maximum gas temperature because of the large heat transfer area available. This provides for long engine life due to low tungsten sublimation rates.

* Contract AF33(616)-8377

II. INTRODUCTION

The Resistojet is an electrically heated rocket. Its existence is made possible by the unique high-temperature capabilities of the refractory metals and hydrogen. In particular, tungsten can be used for a Joule-heated heat exchanger and nozzle. The low molecular weight of hydrogen makes it the optimum propellant in this application.

Spacecraft mission studies conducted by Government and industry groups have revealed a number of very attractive applications for Resistojet propulsion ranging from earth satellite lifting to station keeping and attitude control. The MORL studies are an example of such a promising application (ref.1). The comparative propulsion weight summary of those studies is shown in figure 1. Consequently, substantial research and development support for these devices has been provided by both NASA and the Air Force during the past several years.

The early Resistojet work was primarily undertaken at two laboratories, ASTRO, of The Marquardt Corporation and Lewis Research Center, NASA. The first openly-published reference to the concept was given by Jack (ref. 2) in December 1960. Howard (ref. 3), working concurrently, published early test results in October, 1961. Both designs employed concentric tube heat exchangers. Using hydrogen as a propellant, Howard reported temperatures in excess of 2730°K at heater efficiencies of 86% in the 30 kw class. The Air Force-initiated work at Marquardt began in May, 1961, which was reported by Howard (ref. 4). Later, Jack reported a different heat exchanger concept (ref. 5), using a tungsten wire coil, with early experimental results.

Since that time, a number of groups began work on Resistojets. Many different approaches have been studied. The recent Marquardt-Air Force work on a 30 kilowatt, concentric tube Resistojet, in which thrust measurements were made in a near-vacuum, was reported by Page (ref. 6). The specific impulse was 860 seconds at an overall power efficiency of 0.81. Plasmadyne started with an electrical contact resistance concept, whereby hydrogen was heated as it passed through the rough interface between tungsten plates. The design later incorporated concentric tube features, Todd (ref. 7). AVCO, reported by Bennett (ref. 8), employed several heating techniques, settling on the tungsten wire heater. More recently, John (ref. 9) reported work on small (of the order of watts) Resistojets, using a single tube design. General Electric chose the thermal storage technique for pulsed mode operation. Space Technology Laboratories is now planning to apply a low-powered Resistojet, using nitrogen, on the nuclear detection satellite.

The object of the current program, reported here, was to develop a Resistojet in the 3 kw size from the concentric tube Resistojet technology resulting from the Air Force Program, Page (ref. 6). A number of significant design improvements have been incorporated. Figure 2 shows a sectional drawing of the 3 kw engine.

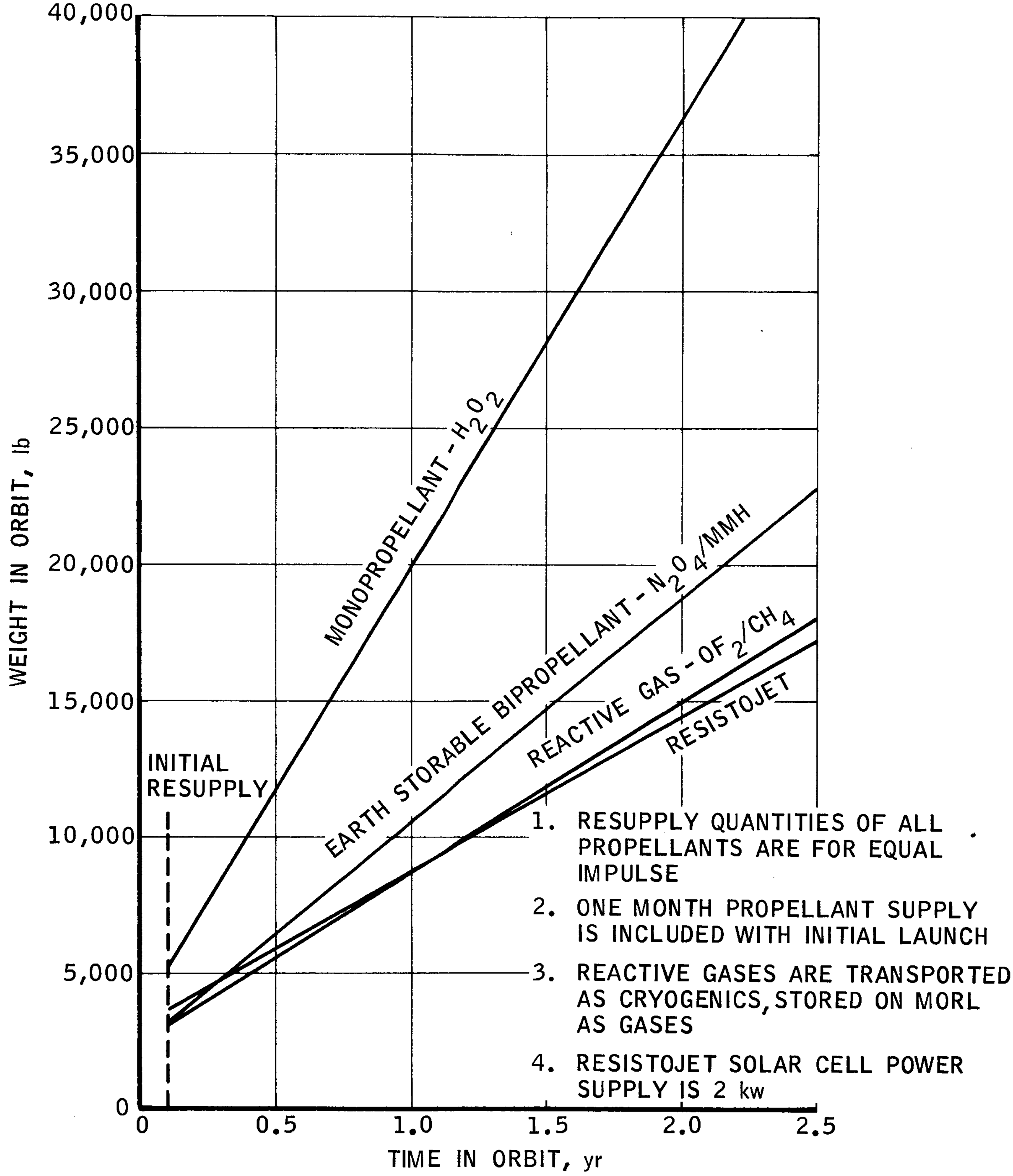

WEIGHT COMPARISON OF PROPULSION SYSTEMS

3 KW CONCENTRIC TUBE RESISTOJET

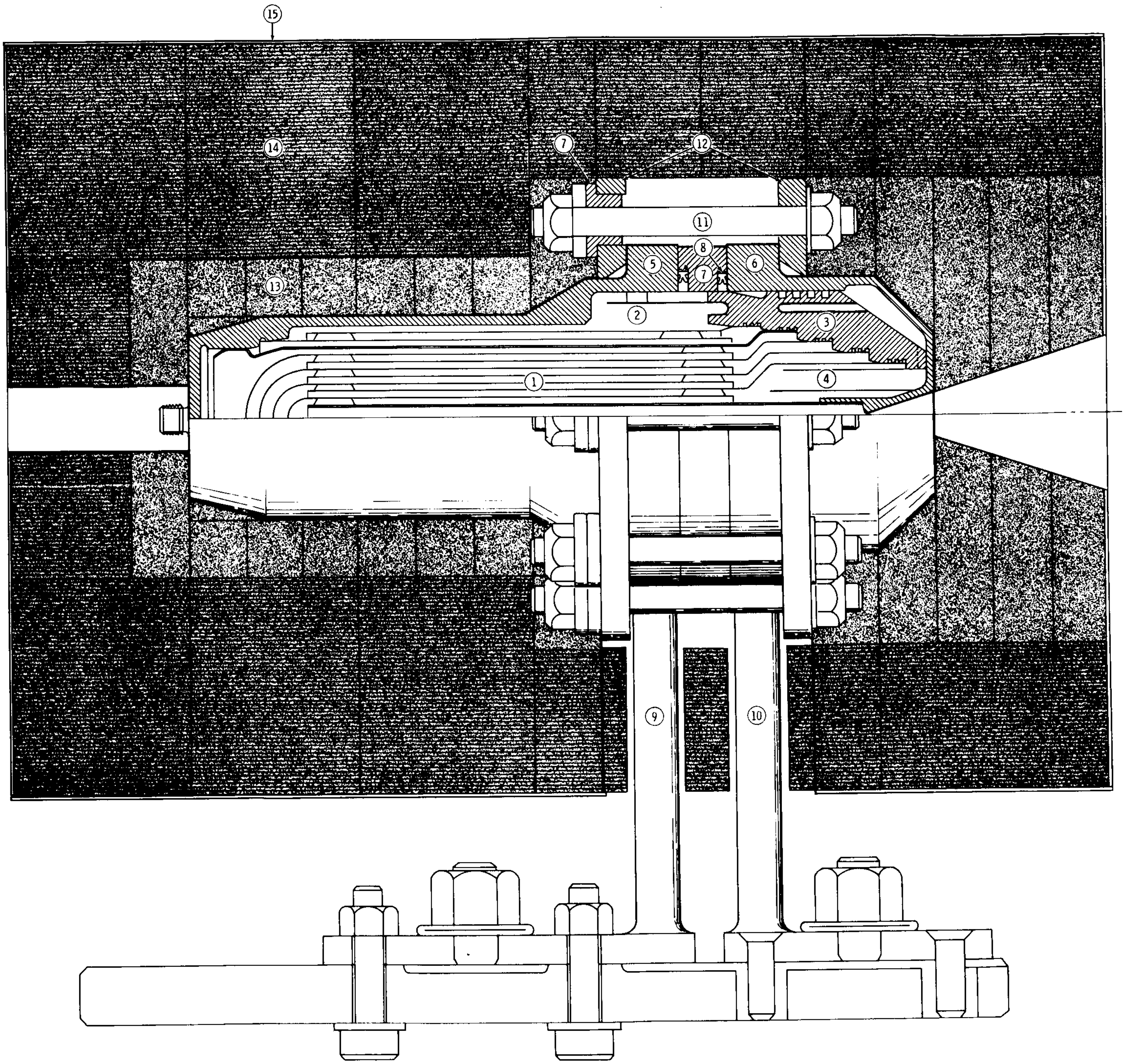

1. I^2R HEATED EXCHANGER TUBES (9) - TUNGSTEN
2. REGENERATIVELY-COOLED SHIELDS (3) - TUNGSTEN
3. HEAT EXCHANGER SUPPORT (ELECTRICAL INSULATOR) - BORON NITRIDE
4. NOZZLE RADIATION SHIELD - TUNGSTEN
5. FORWARD PRESSURE CASE - MOLYBDENUM - 0.5% TITANIUM
6. AFT PRESSURE CASE - TUNGSTEN - 2% THORIA
7. ELECTRICAL INSULATORS - BORON NITRIDE
8. METALLIC FACE SEALS (2) - INCONEL X - SILVER-PLATED
9. ELECTRICAL (+), PROPELLANT FEEDER, THRUSTOR SUPPORT - MOLYBDENUM - 0.5% TITANIUM
10. ELECTRICAL (-), PROPELLANT FEEDER, THRUSTOR SUPPORT - TUNGSTEN - 2% THORIA
11. TIE BOLTS - MOLYBDENUM - 0.5% TITANIUM
12. COLLARS (2) - MOLYBDENUM - 0.5% TITANIUM
13. THERMAL INSULATION - DYNAQUARTZ
14. THERMAL INSULATION - MIN-K-2000
15. CASE -321 STAINLESS STEEL

Figure 2

III. DESIGN BASIS

The analytical basis for the thrustor design, the description and performance of which is given in Sections IV and V, is developed in this section.

From an energy flow viewpoint, the Resistojet involves three energy forms: electrical, thermal and mechanical, in that order. The first conversion is by Joule (resistance) heating, generally an efficient and easily achieved process. The second, that of efficiently converting the thermal energy of the gas into directed kinetic energy (hence thrust), is accomplished with some greater difficulty. The simple appearance of the nozzle is deceptive, as the overall efficiency of the Resistojet under certain circumstances can be dominated by the nozzle process. For this reason, the parameters which affect its performance are considered first.

A. Overall Energy Flow Processes

Figure 3 summarizes the overall energy flow process. This figure illustrates the magnitude and sequence of the loss mechanisms. It further shows the relationship to experimental measurements. The "stream" widths have been made to correspond to measurements made for Point 35.

B. Gas Dynamics

The design of a low thrust nozzle involves minimizing the net losses contributed by the following factors:

a) viscous dissipation or friction
b) lack of complete recombination
c) heat transfer losses from the propellant prior to expulsion
d) momentum lost perpendicular to the thrust direction
e) incomplete expansion in a finite nozzle

The first three losses are size-dependent, being greater for small thrustors. When and to what extent these three factors become important is still a matter of current research.

The loss contribution by each cannot be easily combined to give a net performance figure. However, for a basis of estimation and accounting, the following formula was used:

$$\eta_N = \eta_V \times \eta_D \times \eta_F \times \eta_E \times \eta_T$$

The contributing factors to overall efficiency do interact. An example of this is the effect of the viscous on the frozen flow losses. An overestimation of friction loss causes the chamber temperature required to be calculated too high for a given specific impulse. This in turn increases the frozen flow loss estimate. This was, in fact, the case with the original design estimates.

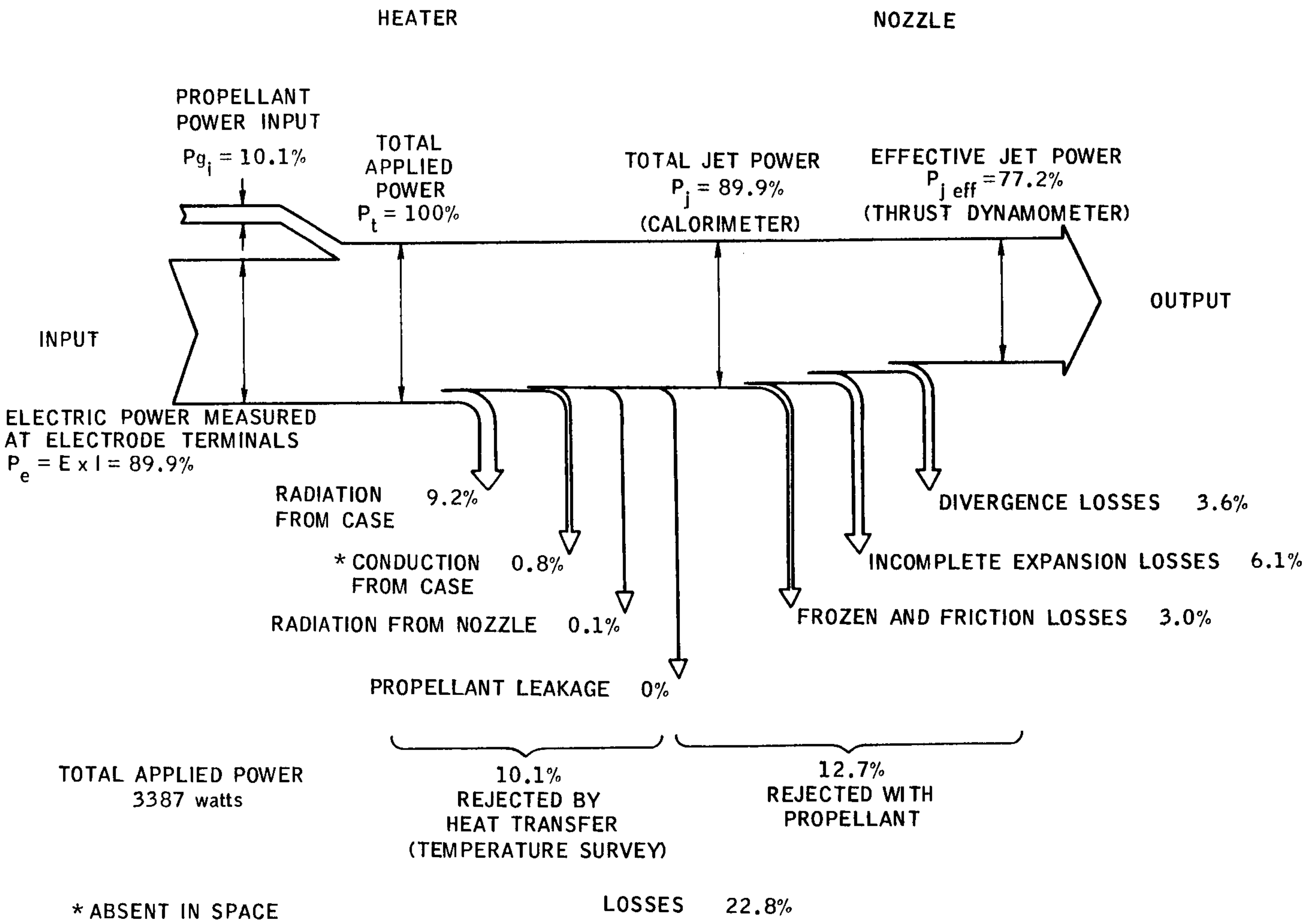

RESISTOJET ENERGY FLOW PROCESS

The loss distribution presented then is based upon the experimental values of overall nozzle performance at Point 35. The observed specific impulse is 828 seconds which corrects to a vacuum value of 838 seconds[1].

1. Frozen Flow Losses.- In nozzle experiments at Marquardt, Oswalt and Widawsky (ref. 10), the performance with hydrogen was found to be closely approximated by equilibrium flow to the throat and subsequent frozen flow thereafter. In any event, even assuming completely frozen flow from chamber conditions at the temperatures required to demonstrate a specific impulse of 828 seconds (2417°K), the frozen flow efficiency η_F is high, namely 0.98 (Spisz, ref. 11). This favorable result is in part due to the high chamber pressure selected.

2. Incomplete Expansion.- The effect of incomplete expansion to a vacuum with hydrogen under frozen flow conditions has been tabulated by Spisz (ref. 11). This gives an expansion efficiency, η_E of approximately 0.94, the exact value depending on the actual effective area ratio. A geometric area ratio of 191 was used on this program in light of the small viscous losses.

3. Divergence Losses.- The divergence, or sometimes called "cosine" losses, have been estimated by several investigators. Under the assumption of spherical flow from a source such as Sutton (ref. 12), a loss of $\eta_D = 0.953$ is estimated for the included half angle of 17.8°. Pitkin (ref. 13), assuming a cosine-like velocity profile produces a divergence efficiency of 0.97. The actual case in light of experimental velocity profiles (ref. 8) is somewhere between the two, or say ~ 0.96.

4. Heat Transfer Losses.- Radiant heat losses from the nozzle were measured to be negligible. Any convective losses were returned to the heat exchanger element. This term was ignored.

5. Viscous Losses.- The original viscous loss estimates were based upon the viscous nozzle studies of Pitkin (ref. 14). The experimental coefficients used in that analysis were based upon the data of Tinling (ref. 15), which is currently undergoing re-evaluation.

The current program results indicate that the viscous losses are not severe. The Reynolds number based upon throat diameter was 3750.

The calculated viscous losses on the basis of a boundary layer and inviscid core give $\eta_V = 0.95$. This is lower than that calculated from the experimental results by the difference method which gives $\eta_V = 0.99$. However, the total experimental error is prominent in this difference, so no great quantitative confidence can be placed in its value. In summary, the various loss factors that contribute to nozzle efficiency are shown as table I.

(1) See page 62 for correction to space vacuum operation. This correction was necessary here to account properly for the loss distribution.

TABLE I.- Estimated Nozzle Loss Distribution (Data Point 35)

Frozen flow	0.98
Divergence losses	~ 0.96
Incomplete expansion	~ 0.94
Friction	0.99
Overall Nozzle	0.88

6. Nozzle Geometry.- Based upon the nozzle studies of Pitkin (ref. 14), the nozzle of the geometry shown in figure 4 was chosen.

The nozzle discharge coefficient, C_D, which represents the effective to geometric throat area ratio was taken from Simmons (ref. 16). The coefficient was estimated to be 0.91.

C. Heat Transfer

1. Heat Exchanger.- The temperature distribution and the heat flow through the heat exchanger were calculated for the 30 kw Resistojet using a thermal analyzer program. This program, written for the IBM 704 computer, solved a thermal resistance network of some 200 nodes for all three heat transfer modes (ref. 4). Although an exact solution to the Resistojet problem is not possible, the program offers a good approximation of the temperature distribution through the thrustor. In view of the similarity of the 3 and 30 kw engines, a complete 3 kw analysis was not necessary. The results of the 30 kw analysis were modified to account for the differences in size, insulation and shielding between the two engines.

Figure 5 shows the estimated temperature distribution of the successive tungsten elements and the hydrogen temperature from inlet to discharge. The abscissa is presented in terms of pass lengths. Note that a given heat exchanger element is presented twice as it represents the inner wall on the initial pass and the outer wall on the succeeding pass of the hydrogen.

The flow throughout the heat exchanger is laminar. In the first pass the Reynolds number is 1750, and at exit just prior to the nozzle entrance, it is 600. The maximum velocities are low, approximately 50 meters per second; the Mach number is very low, namely ~ 0.014.

Some of the parameters of interest with regard to the heat exchanger are shown in table II.

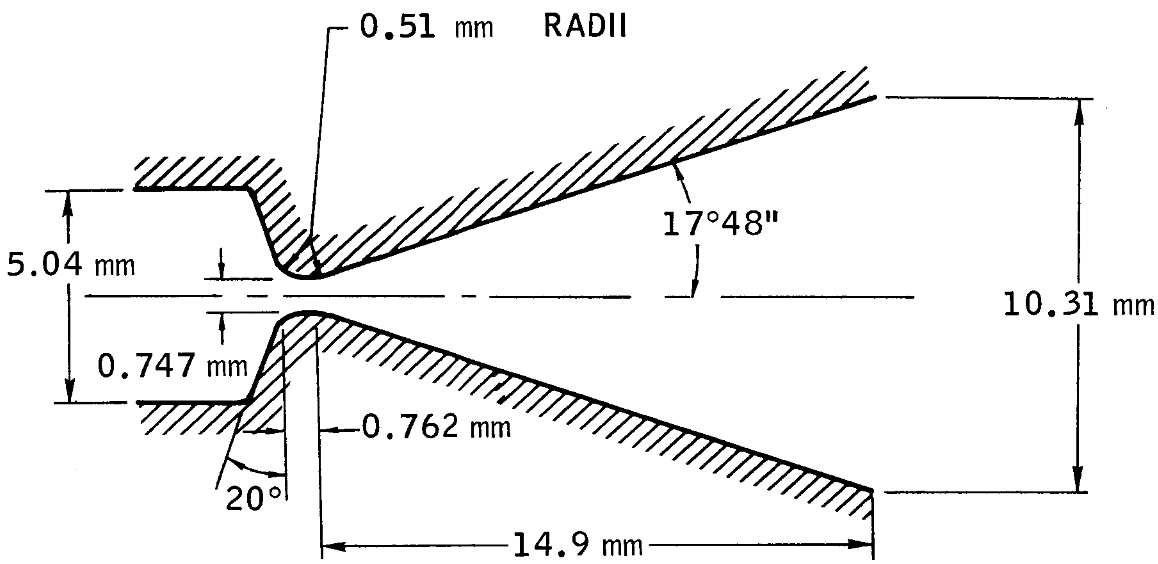

AREA RATIO = 191:1

NOZZLE DESIGN SUMMARY

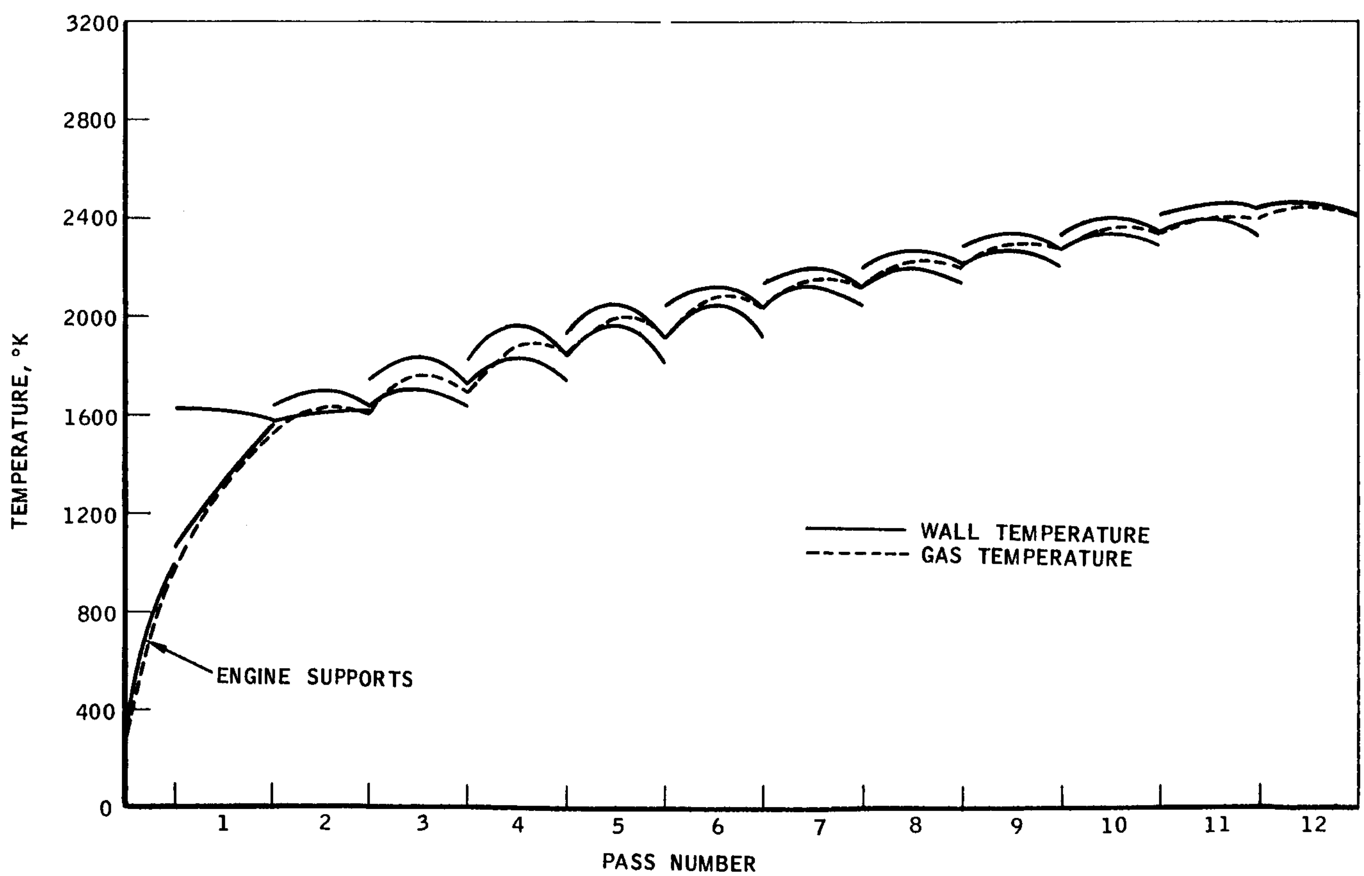

ESTIMATED HEAT EXCHANGER TEMPERATURE DISTRIBUTION

R-19,969

Part No.	Element	Inside Diameter cm	Radial Spacing cm	Thickness cm	Physical Length cm	Cold Resistance ohms	Material and Fabrication Method
X8021-3	Heater	0.4763		0.014	12.159	0.00301	Vapor deposited tungsten
			0.1448				
X8021-5	Heater	0.7938		0.013	9.538	0.00150	Vapor deposited tungsten
			0.1461				
X8021-7	Heater	1.1113		0.011	13.175	0.00107	Vapor deposited tungsten
			0.1473				
X8021-9	Heater	1.4288		0.010	9.853	0.00084	Vapor deposited tungsten
			0.1485				
X8021-11	Heater	1.7463		0.010	12.383	0.00068	Vapor deposited tungsten
			0.1485				
X8021-13	Heater	2.0638		0.010	10.171	0.00058	Vapor deposited tungsten
			0.1485				
X8021-15	Heater	2.3813		0.010	11.590	0.00050	Vapor deposited tungsten
			0.1485				
X8021-17	Heater	2.6988		0.010	10.488	0.00044	Vapor deposited tungsten
			0.1485				
X8021-19	Heater	3.0163		0.020	12.852	0.00039	Vapor deposited tungsten
			0.1378				
X8022-3	Shield	3.3325		0.025	10.160	--	Vapor deposited tungsten
			0.1334				
X8022-5	Shield	3.6500		0.025	10.000	--	Vapor deposited tungsten
			0.1334				
X8035	Forward Case	3.9675		--	8.412	--	Cold machined - ½% titanium, molybdenum
					Total-	0.00901 ohms	

Heat Exchanger Description

Table II

A significant characteristic of the solution is that the gas approaches the maximum wall temperature requiring little over-temperature, as was experimentally verified (ref. 17). This is one of the definite advantages of the concentric tube design, in that a higher specific impulse may be achieved at less expense in terms of engine life.

2. Insulation.- In the 30 kw design, the heat losses from the engine case amounted to about 5% of the input power. On the 3 kw design, however, the exterior radiating area is not appreciably smaller, yet the operating temperature would be expected to be similar. This would mean that a larger percentage of the input power would be lost by radiation from the outer shell. Radiation shields around the heat exchanger and a thick layer of insulation around the pressure case were provided to reduce these losses (see fig. 2). The inner insulation assembly consists of Dynaquartz, which has a thermal conductivity of 1.73×10^{-3} watt/cm°C and a maximum temperature capability of 1510°C. The exterior layer of Min-K 2000 possessed a lower thermal conductivity one-third that of Dynaquartz, but was limited to use in the regions where less than 1093°C was anticipated. The overall heat loss from the engine was calculated to be 10% of the applied power. This was verified in subsequent testing. The conductive heat transfer through the insulation compared closely with the calculated radiation loss from the outer stainless steel shell.

An interesting feature is that, although the power is generated primarily in the smallest tubes, it is transferred to the gas to the greatest extent in the first few passes. This is due to the large radiant heat flux in the radial direction. Little heat is lost through the engine supports since the incoming propellant carries most of this thermal leakage back into the engine. Note that a significant percentage of the gas heating takes place in these supports.

D. Electrical Parameters

The thrustors being actively developed today are generally electrically incompatible for direct connection to the space power sources under development. Resistojets appear to be the one exception to this trend.

The Resistojet appears to the power supply as a resistance with a negligible capacitance (less than 0.1 picofarads), and inductance (less than 0.01 microhenries), hence under steady conditions it can be operated directly from either an A.C. or D.C. constant voltage power supply without the need for power adaptation devices. Only the starting characteristic requires special consideration, since the hot resistance is about eight times the cold value.

The present study requires Resistojet compatibility with a solar cell power supply, consisting of series-connected cells which are considered to yield a maximum continuous voltage up to 56 volts.

The concentric tube heat exchanger allows latitude in the selection of operating voltage. The considerations of (1) heat transfer and (2) decreased life due to sublimation dictate the geometry of the heat exchanger and thus the "nominal" design voltage. The first sets the surface area (i.e., diameters, lengths, and number of elements); the second the element thickness. The "nominal" design electrical resistance is thus prescribed. Choosing to decrease the design voltage from the nominal value only involves increasing element thickness, a minor change. Choosing to increase the design voltage involves increasing the electrical path length. This is done by raising the number or length of the elements. The first generally does not involve increasing the package envelope and is more desirable from a heat exchanger efficiency viewpoint.

The operating voltage of the engine at 3 kw, after the apparent diffusion bonding, stabilized at 15.4 volts. See table II for the associated heat exchanger element thicknesses and figure 5 for the temperature distribution. For the same specific impulse of 828 seconds, a 30 kw Resistojet would operate at 50 volts at design (ref. 17). These may be considered the "nominal" design voltages. For systems compatibility purposes, the terminal voltage may be changed upward approximately forty percent by doubling the number of elements, and reduced thirty percent by doubling element thicknesses over nominal. Figure 6 shows the approximate design range. This family has identical thrustor performance differing only in electrical characteristics.

E. Mechanical Considerations

1. Seals.- The concentric tube configuration requires an electrical insulator in its pressure case. For this engine, mechanical seals were used to provide ease of disassembly for development purposes. Later flight hardware could be sealed by a ceramic-to-metal bond type insulator.

The location and cross-sectional geometry of the seal area is shown in figure 2. Two metallic seals are necessary. The insulator shown is made of Type HBR boron nitride. The metallic static face seal used was manufactured by the Haskel Engineering and Supply Company, Burbank, California. It was the HS-4 series standard. This is an Inconel-X, K-type seal which is silver-plated. The temperature rating of the Inconel-X is 650°C for continuous service, and the silver-plating is 900°C. The seals work on the principle of internal pressure loading to increase the sealing lip pressure. The surfaces of both the forward molybdenum case and aft tungsten case were hand lapped to a mirror finish, 8 rms, and the boron-nitride mating surfaces to a smooth finish.

The bolted joint is designed to apply a compressive load on the seals through proper selection of materials and dimensions. A boron-nitride electrical insulator is included on the tie bolts for two purposes. The first is to provide electrical separation, and the second is to be a flexible spring so as to unlock any possible thermal stresses in the seal members.

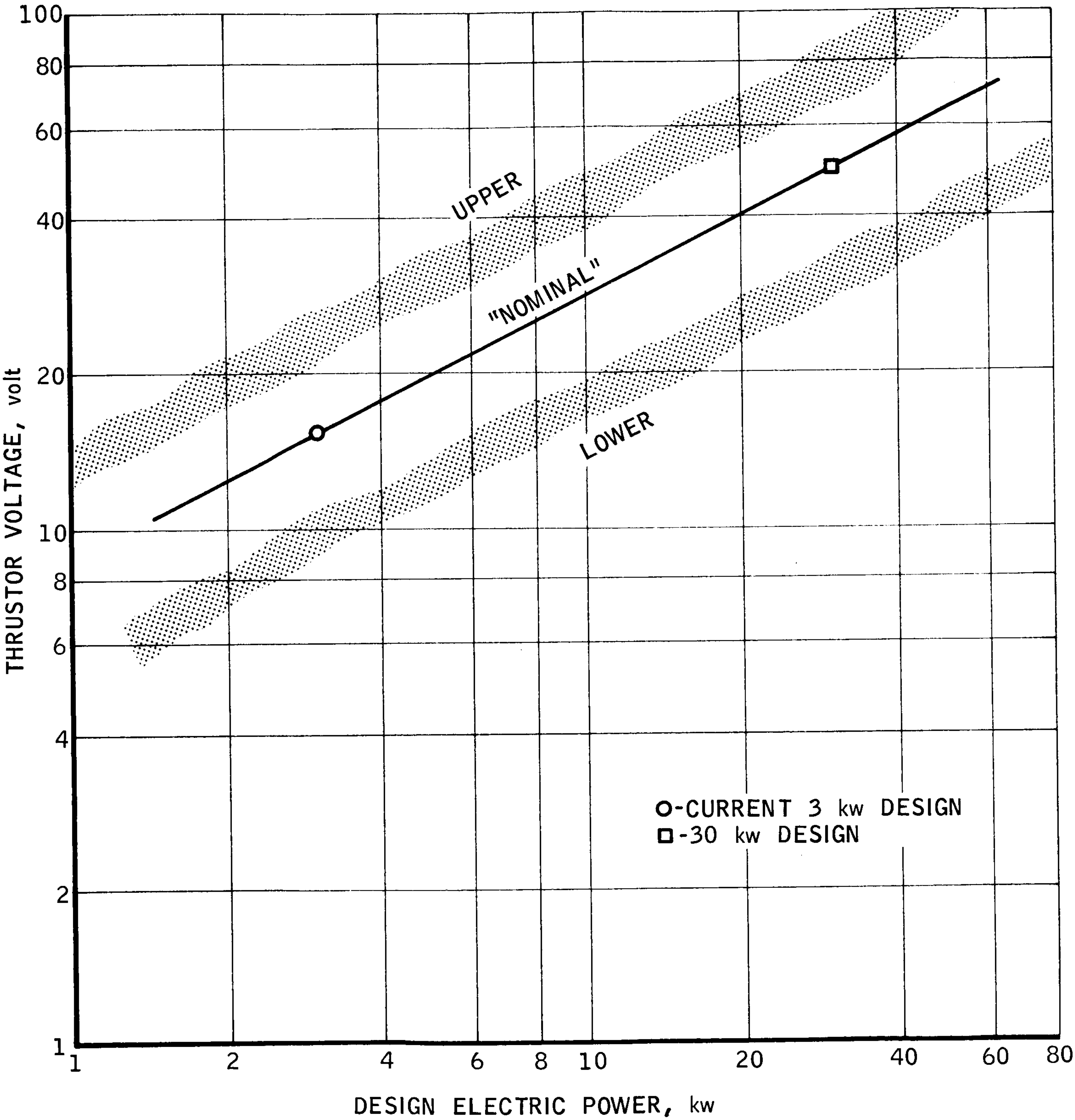

APPROXIMATE DESIGN RANGE OF THRUSTOR VOLTAGE

HS-4 seals made of special material, Rene' 41, were ordered. These have a temperature capability of 926°C and are gold-plated for a plating temperature capability of 1010°C. These seals were unavailable during the test program, but will be shipped with the engine to the Lewis Research Center and employed for the endurance test.

2. Thrustor Supports.- Figure 7 shows the two multi-purpose thrustor supports. These supports serve as (a) the propellant feed to the engine, (b) electric power terminals, and (c) engine supports with minimal thermal leakage.

3. Boron-Nitride Parts.- Hot pressed boron nitride was selected for the electrical insulators on the case bolts and between the fore and aft cases. It was also used to provide a support for the heat exchanger. Boron nitride has good strength properties at elevated temperatures as long as it is not exposed to extremely high temperatures.

Type HBN boron nitride was used for the heat exchanger support because of its thermal expansion properties. Type HBR was used for the other parts because it is less hydroscopic and therefore requires no baking before use. Type HBR also has better strength properties but a larger thermal expansion coefficient than HBN. The latter rendered it unsuitable for the heat exchanger support.

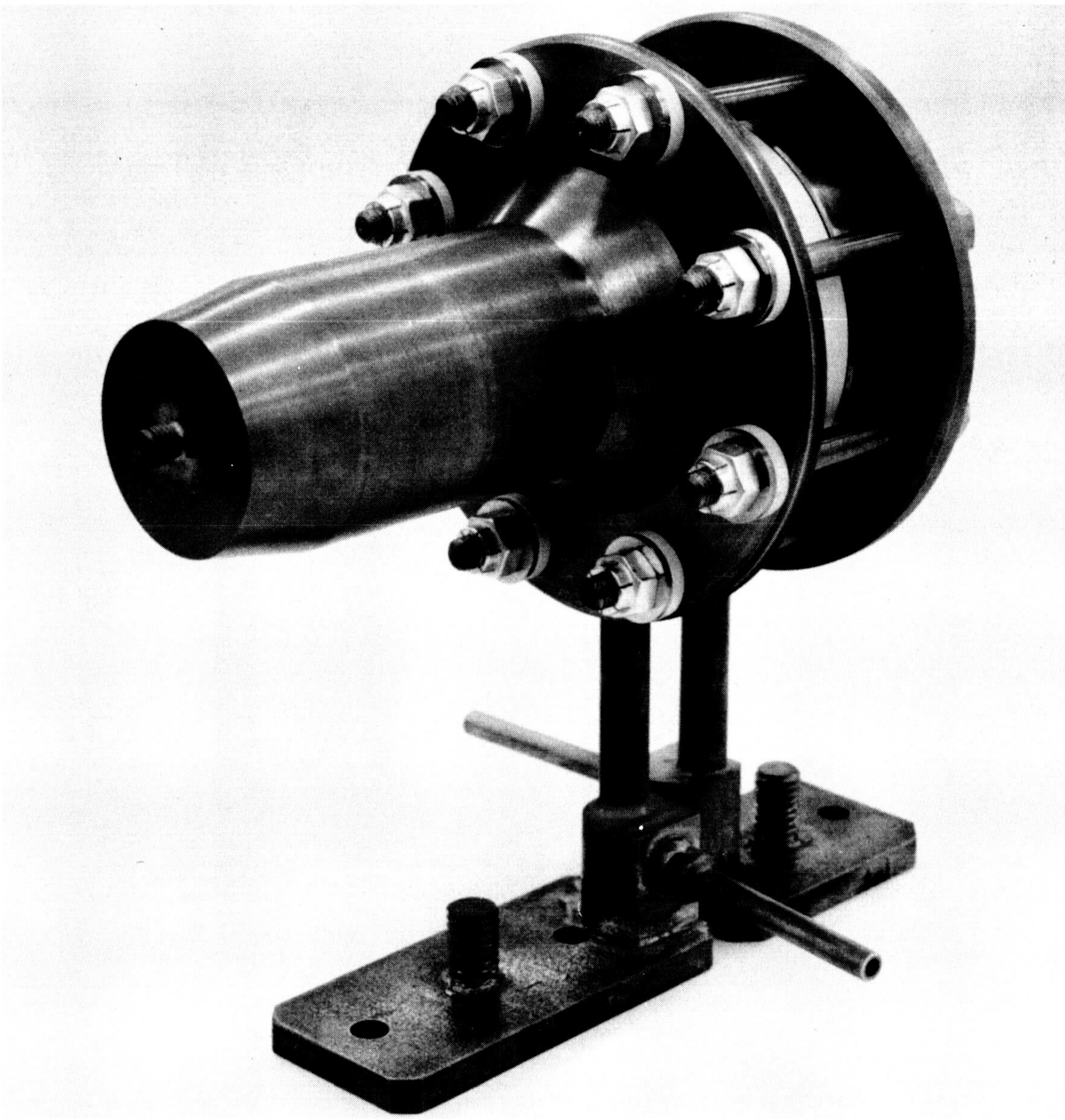

THRUSTOR ASSEMBLY LESS INSULATION

IV. DESCRIPTION

A. Physical Description

In previous concentric tube Resistojet engines, the heat exchanger tubes were cylinders formed from rolled tungsten sheet and electron-beam welded along the seams. These tubes were supported and sealed at both ends by boron-nitride supports and electrically connected by corrugated strips placed between the concentric tubes.

Since boron nitride has been a source of trouble in previous designs, an attempt was made to place it in a cooler environment in the 3 kw engine. Domed ends were provided on alternate tubes at the upstream end so that the exchanger needed a seal at only the downstream end. The ends of the tube which rest in the BN heat exchanger support were flared and lengthened to place them in a cooler environment; and a labyrinth seal is provided to prevent short-circuiting of the gas path. The tubes are held concentric and connected electrically by small integral struts which were made possible by the vapor deposition process which also provided the domed ends and flares. See figure 8.

Figure 9 shows the boron nitride heat exchanger seal and support with the large shield added as a design change to protect the seal area (top), and the small shield designed to protect the BN (partially withdrawn from BN).

A majority of the thrustor parts, with the exception of the insulation, outer shell, and some nuts and washers, are shown in figure 10. Note that the boron-nitride part shown does not incorporate the modification mentioned above.

Figure 11 shows the insulation and stainless steel outer shell which surround the engine.

B. Fabrication

1. Heat Exchanger.- Fabrication of the heat exchanger tubes and shields was done by vapor-depositing tungsten on the exterior of molybdenum mandrels (fig. 12). The coatings were precision-ground at mating surfaces and the mandrels were chemically removed, leaving the desired thin-walled elements.

The elements were assembled with interference fits and were diffusion-bonded during the test.

The various vapor-deposition techniques are described in references 18 and 19. Additional development effort was required to produce the heat exchanger successfully used here. This was done in cooperation with the San Fernando laboratories.

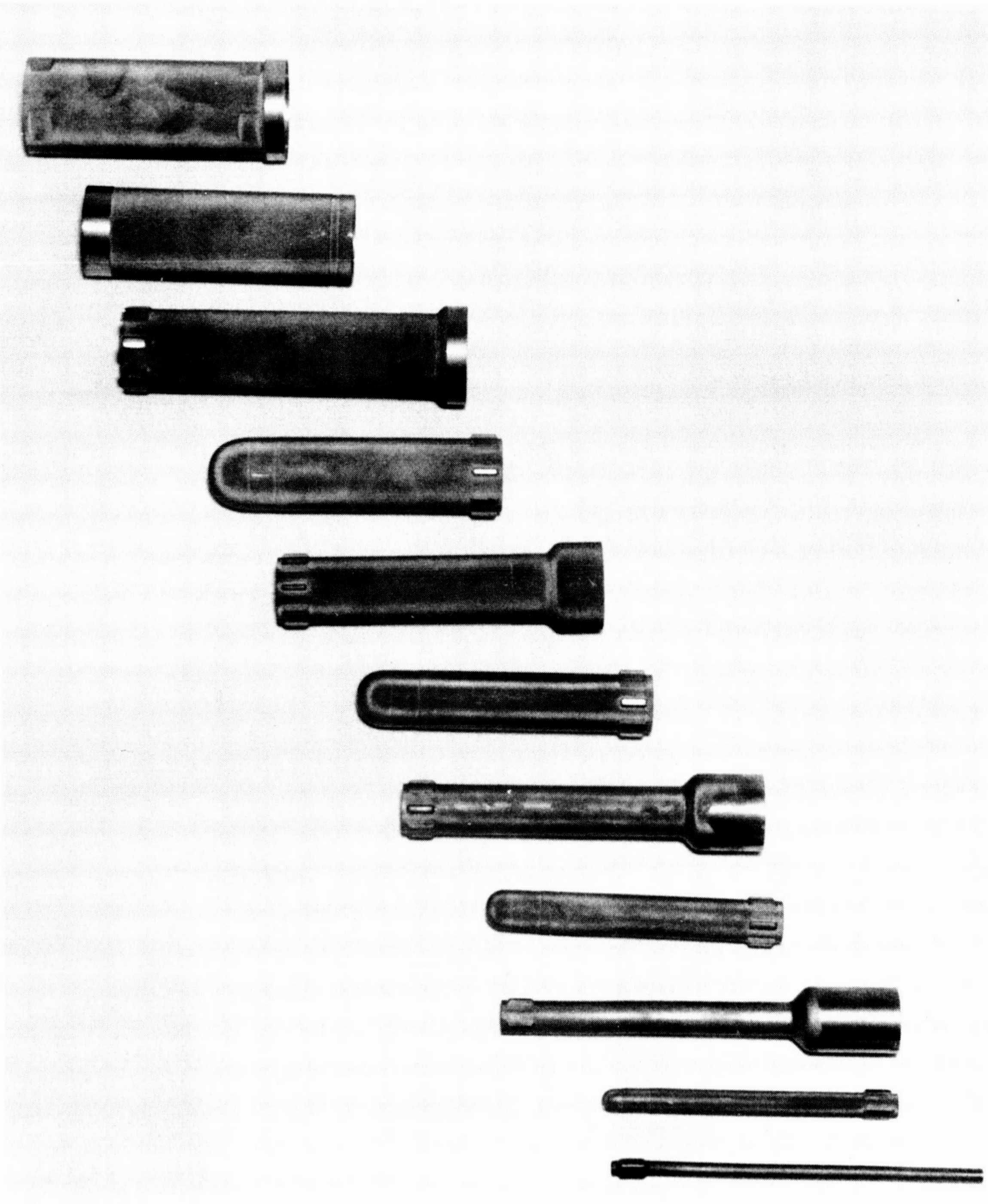

TUNGSTEN HEAT EXCHANGER TUBES AND SHIELDS

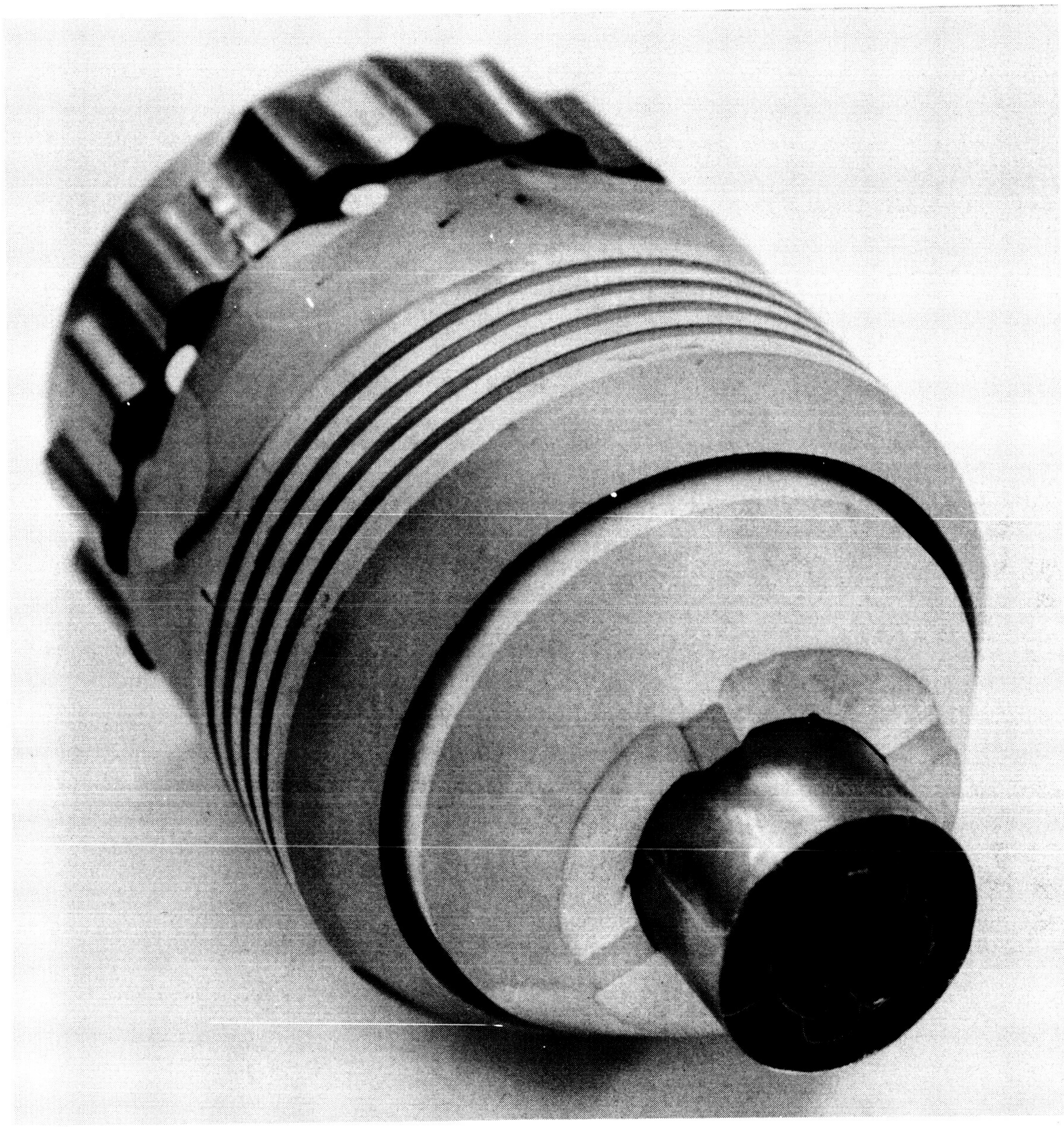

BORON NITRIDE HEAT EXCHANGER SUPPORT
AND RADIATION SHIELDS

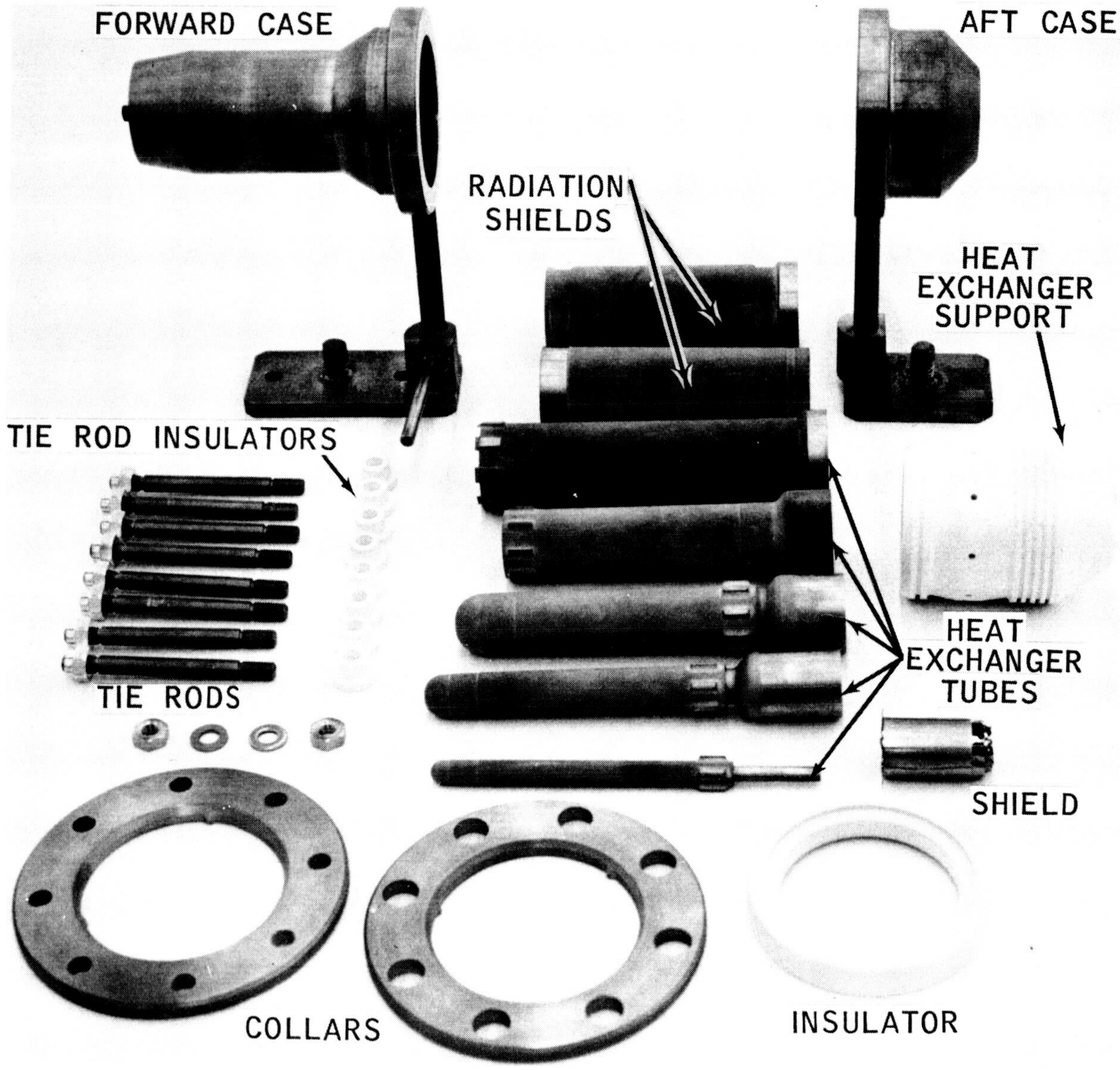

3 KW RESISTOJET PRIOR TO ASSEMBLY

R-19,946
Neg. 6627-1

Figure 10

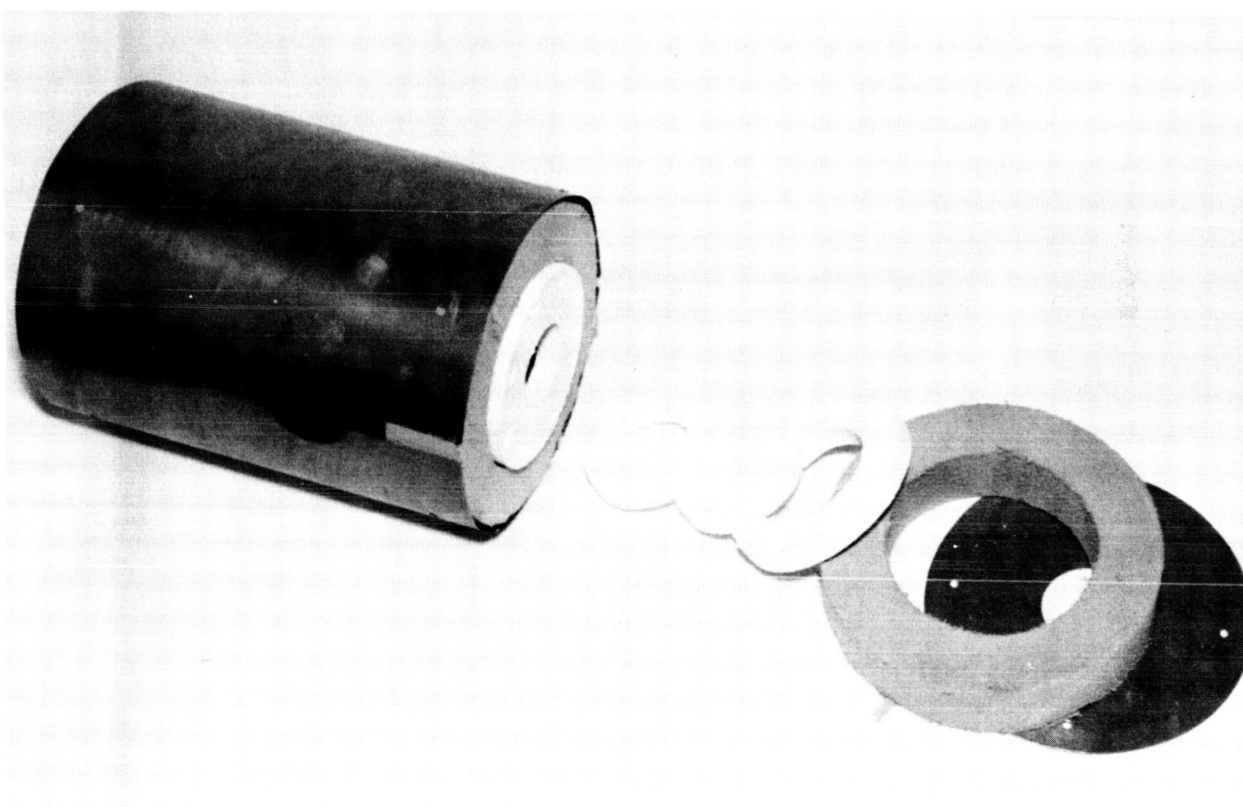

INSULATION ASSEMBLY

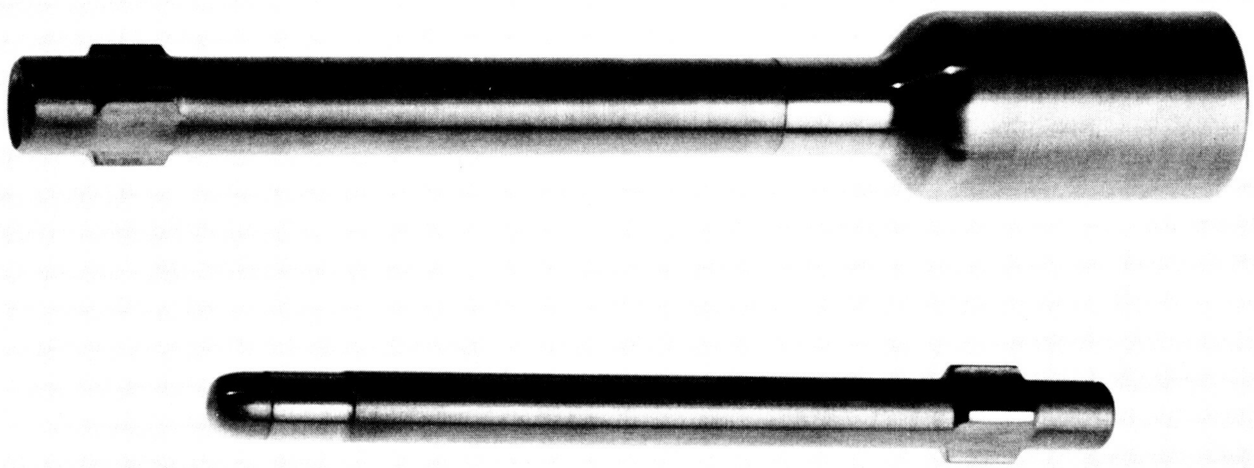

MOLYBDENUM MANDRELS FOR VAPOR DEPOSITION
OF TUNGSTEN HEAT EXCHANGER TUBES

R-19,972
Neg. 6476-I

Initially, a one-piece heat exchanger concept was considered. This was rejected as piece-by-piece addition of tubes was still found necessary with a single error possibly ruining the whole assembly.

Five features of the tubes which required development were: 1) uniformly thin walls ($\sim$ 0.01 cm), 2) hemispherical domed ends, 3) integral struts (for support and electrical continuity between elements), 4) flared transition section, and 5) precision joint dimensions. All but the last was solved in the vapor-deposition process itself. The last was solved by precision-grinding of the tubes while on the mandrels.

Tungsten is deposited on the mandrel according to the equation

$$WF_6 + 3H_2 \longrightarrow W + 6HF$$

The mandrel, located in a cylindrical chamber 1 cm larger in diameter than the part, is subject to an axial flow of pre-mixed tungsten hexafluoride and hydrogen for 15 minutes. The mandrel is rotated at 5 rpm and subjected to induction heating to 700°C. Chamber discharge pressure is maintained at 250 mm Hg by pumps.

The deposit tends to vary in thickness near indentations and protrusions. This required some trial shapes. For better strength, male struts were finally employed, rather than the female type originally tried.

If an insufficient thickness of tungsten is applied, a second coat may be deposited on the first with no adhesion problems. It was desirable, however, to achieve the required thickness with one application, so a slight excess was deposited and then the joining parts of the tubes were ground to the appropriate dimensions. In this operation it was found that dimensions could be held within one ten-thousandth of an inch. This precision-grinding made possible the slight interference fits which provided the necessary pressure for diffusion-bonding, discussed below, without cracking the tubes. The tubes were ground before removing the mandrels in order to give all possible support to the thin walls during the grinding operation.

Mandrel removal was done chemically with a mixture of HCl and HNO_3, which vigorously attacks molybdenum without noticeable reaction with tungsten. Axial holes were made in the mandrels before vapor-deposition to provide a larger surface on which the acid could work and thus speed the removal process.

The choice of mandrel material is an important one since it must match the deposited tungsten quite closely in thermal expansion coefficient. After cooling, a dissimilar material would either crack the tube or pull away from it. The latter would make grinding of the tube on the mandrel impossible. The choice of 0.5% titanium-molybdenum proved very successful. This material, however, because of the difficulty in precision-machining, added considerably to the expense of engine fabrication.

2. Element Bonding.- Because of the difficulties that would be involved in trying to braze an assembly of tubes suitable for high-temperature service, the Resistojet heat exchanger was designed to join its tubes by diffusion-bonding while in the test chamber for reasons of speed and economy. This bond gives a temperature capability equal to that of the parent metal. In production the tubes would be bonded electrically in a special furnace prior to test to insure immediate electrical stability.

In an ordinary contact between two metal surfaces, the actual contact area is much smaller than the surface area in "apparent" contact. This is due to the microscopic irregularities in the surface so that, in effect, the metal surfaces touch only at the high points. The forced constriction of current flow through these small paths is the cause of the resistance at a contact (ref. 20).

Due to the high current density at the contact points, a relatively large quantity of heat is generated in the contact region. The radial temperature gradient in the exchanger with subsequent joint over-temperature causes an increased pressure to be applied by the interference fit. These conditions of temperature, pressure and time between refractory metal surfaces in the presence of hydrogen have produced diffusion-bonding in separate Marquardt tests (ref. 21).

The elements did bond under test conditions (see Section V.B). When the engine was disassembled after the test, only three of the ten joints could be separated; the others seemed quite firm.

3. Braze Joints.- The various joints in the engine supports and propellant feed lines caused some difficulty initially. Because these joints had to be hydrogen-tight at a pressure of ten atmospheres, brazing was chosen as the only technique with a good chance of success. The original configuration of the joints consisted of molybdenum supports for both the forward and aft cases. Molybdenum fittings were inserted into the support tubes and stainless-steel tubes were inserted into the fittings. The braze material chosen was Coast Metals 62 containing 67% manganese, 16% nickel, 16% cobalt and 1% boron. Mo-Mo and Mo-W sample joints were successfully made with the above filler material. The only joint in which the braze material did not crack was the Mo-Mo joint between the support tube and the forward case. Analysis showed that the Mo-W and stainless-to-molybdenum joints cracked because the differences in thermal expansion coefficients allowed the joined members to pull the braze material apart on cooling. The material for the aft case support was changed to 2% thoriated tungsten to match the case. Also the inlet tube-to-support joints were changed to provide stainless-steel outer members and therefore compression of the filler material during cooling. The joints were brazed again, this time in an inert atmosphere with Coast Metals 62, and were found to be leakfree when tested with a helium leak detector. After the second aft case was cracked during the initial assembly attempt, it was found that a good Mo-W joint could be made using Permabraze 130, 82% gold and 18% nickel. This was used to repair the first case assembly which was subsequently used for the 25-hour test.

4. Assembly of the Engine.- The heat exchanger tubes were first assembled in pairs beginning with the two smallest tubes. This required a certain amount of side-to-side motion combined with a steady pressure. Next, the insulating support and nozzle shield were positioned in the aft case assembly and the pairs of tubes were fitted into the support. The largest heat exchanger tube and the two shields were assembled and fitted into the forward case. The other radiation shield was then added.

The width of the outside ring of each k seal was measured and the seals and insulator were then positioned. The gaps between each case section and the boron-nitride insulator were measured and recorded. The tie rods and accompanying hardware were assembled and slowly tightened with a torque wrench until the gap measurements indicated that the outside rings of the k seals were bottomed.

The base was bolted to the engine and a leak check made. The thrustor was pressurized with hydrogen at 20 psig for several minutes with no noticeable leaks. Thermocouples were attached at the points shown in figure 13, and the insulation and outer case were then added.

Leak checks were made under a bell jar at chamber pressures of 50 and 100 psia using hydrogen. Leak rates were less than 4×10^{-5} gram/sec or less than 0.05% of the actual mass flow.

TEMPERATURE SURVEY OF LABORATORY UNIT

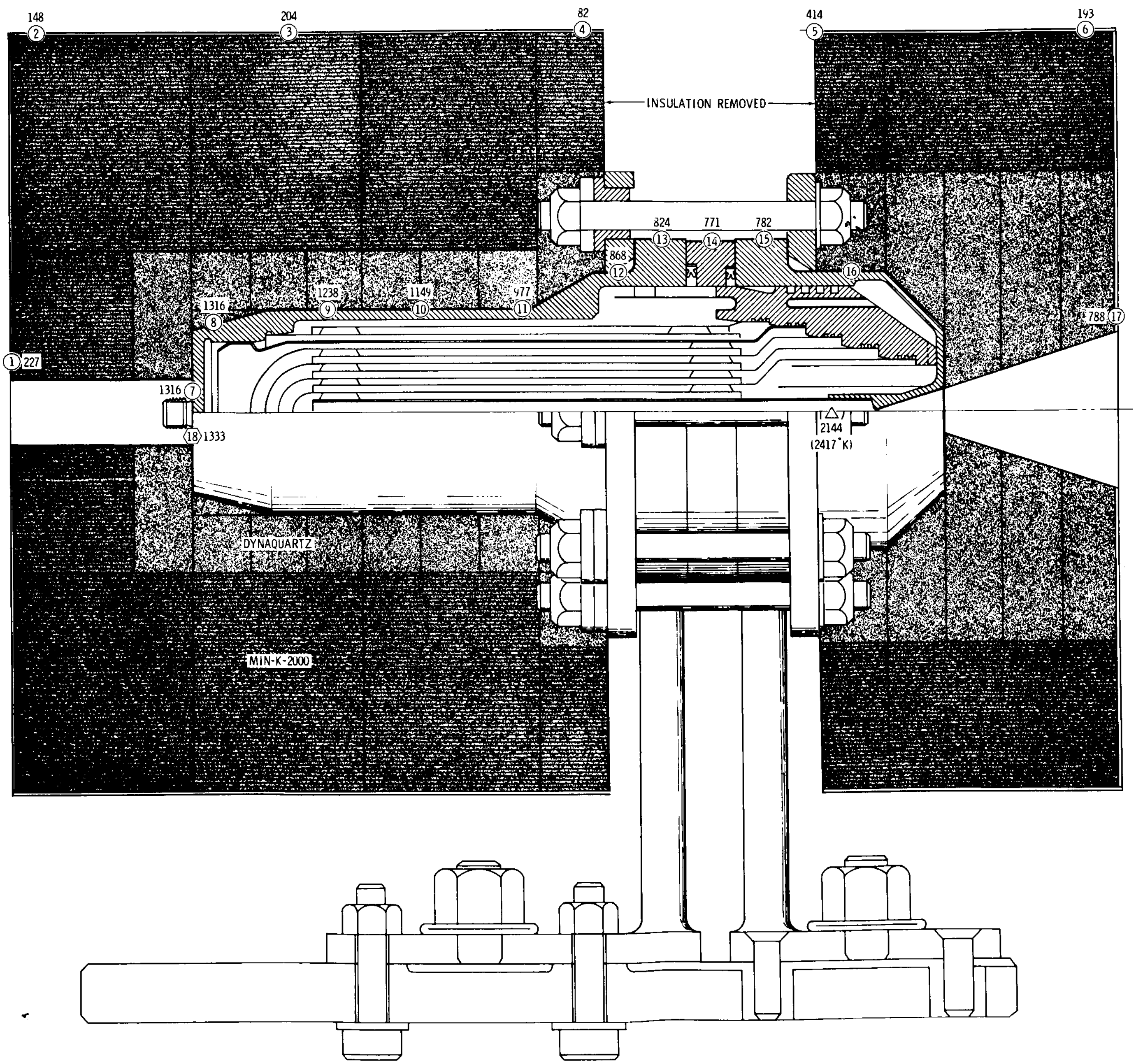

SOURCE:

◯ C. A. THERMOCOUPLES

⬡ OPTICAL PYROMETER

△ ENERGY BALANCE

OPERATION:

SPECIFIC IMPULSE = 828 sec

POWER = 3.05 Kw

MASS FLOW = 7.93×10^{-2} g/sec

(NOTE: TEMPERATURES IN °C)

R-19,004B

Figure 13

Drawing No.	Part	Material
X8021	Heat Exchanger Assembly	Vapor deposited tungsten
X8022	Shield Assembly	Vapor deposited tungsten
X8023-3	Insulating Support	Boron nitride (type HBN)
X8023-5	Radiation Shield	Tungsten sheet
X8024	Nozzle Shield	Tungsten sheet
X8025-3	Case Support	Molybdenum, ½% titanium
X8025-9	Propellant Tube	321 Stainless steel
X8025-11	Adaptor	321 Stainless steel
X8026-3	Case Support	Tungsten, 2% thoria
X8026-11	Adaptor	321 Stainless steel
X8026-13	Propellant Tube	321 Stainless steel
X8027	Insulating Spacer	Boron nitride (type HBR)
X8028	Forward Collar	Molybdenum, ½% titanium
X8029	Aft Collar	Molybdenum, ½% titanium
X8030	Tie Rod	Molybdenum, ½% titanium
X8031	Insulating Bushing	Boron nitride
X8033	Thrust Washer	321 Stainless steel
X8034	Aft Case	Tungsten, 2% thoria
X8035	Forward Case	Molybdenum, ½% titanium
X8067-3,-5,-7	Outer Insulation Shell	321 Stainless steel
X8067-9	Outer Insulation	Min-K 2000
X8067-11	Forward Inner Insulation	12 lb. density Dyna-Quartz
X8067-13	Aft Inner Insulation	10 lb. density Dyna-Quartz

MATERIALS SUMMARY

TABLE III

V. PERFORMANCE

Development testing of the concentric tube Resistojet began on 23 March and culminated in a successful 25-hour performance test on 2 May 1965. The thrust simultaneously exceeded the contract-specified values of specific impulse and overall efficiency as shown in table IV. Post-test inspection showed the engine to be in excellent condition.

Table IV.- Performance Comparison

	Contract (1)	25-hour Performance Test
Electric power, P_e, watts	3,000	3,044
Specific impulse, I_{sp}, sec	--	828
Specific impulse in vacuum, $I_{sp_{vac}}$, sec	$>$ 800	838
Total Power efficiency, η_o	0.65	0.772
Electric Power "efficiency", η_o^*	(0.715)	0.860
Mass flow, $\dot{m}$, gm/sec	(0.0698)	0.0793
Thrust, F, gm-force	(55.8)	65.7
Thrustor total gas temp., °K	(2740)	2,417
Thrustor chamber pressure, atm.	(10)	8.79
Cell pressure, mm-Hg	--	0.7
Propellant inlet basis temp., °C	(30)	30

The performance of the Resistojet was steady during the test with one anticipated exception. The electrical characteristics changed at 18 hours due to tube joint bonding. This was accomplished in the test cell rather than in a furnace for economy reasons, as pointed out in Section IV.B. The data are summarized in the figures that follow and detailed in the ensuing text.

(1) Values shown in parentheses are derived based on the conditions specified by contract at a propellant inlet temperature of 30°C.

Test Date 23 April 1965

Point No.	Electrical Power watts	Total Power watts	Thrust grams	Measured Specific Impulse sec	Observed Overall Total Power Efficiency %	Heater Efficiency %
1	0	321	19.8	265	78.5	100
2	32.7	353.7	20.2	270	74.3	100
3	126.8	447.8	22.6	302	73.3	99.9
4	277	598	26.2	350	73.8	99.8
5	499	820	30.1	402	71.1	99.5
6	707	1028	35.6	476	79.3	99.4
7	946	1267	38.8	519	76.4	99.2
8	1178	1499	42.2	565	76.3	98.7
9	1603	1924	47.4	635	75.4	98.2
10	1785	2106	49.7	665	75.4	97.5
11	2008	2329	51.8	693	74.2	96.5
12	2310	2631	55.4	741	75.2	94.5
13	2495	2816	57.6	771	75.8	91.7

Note: Hydrogen Flow - .0748 gram/sec.

DATA SUMMARY
TABLE V

Test Dates 30 April to 2 May 1965

Point No.	Electrical Power watts	Total Power watts	Thrust grams	Mass Flow gram/sec	Measured Specific Impulse sec	Observed Overall Total Power Efficiency %	Heater Efficiency %
1	0	323.5	20.5	.0748	274	83.6	100
2	278.5	602	26.1	.0748	349	72.6	99.4
3	488.5	813	31.0	.0748	414	75.9	99.1
4	760.0	1084	36.2	.0748	484	77.7	98.7
5	1011	1335	40.7	.0748	544	79.9	98.2
6	1153	1477	42.5	.0748	568	78.6	98.0
7	1593	1917	47.4	.0748	634	75.5	97.4
8	2021	2345	51.7	.0748	691	73.3	96.0
9	2256	2580	54.0	.0748	722	72.7	95.0
10	2499	2823	56.6	.0748	757	73.0	92.7
11	2538	2882	60.5	.0793	763	77.0	92.4
12	2747	3091	62.6	.0793	789	76.9	91.4
13	2907	3250	63.4	.0793	799	75.0	91.2
14	3026	3369	63.9	.0793	806	73.5	91.1
15	3044	3387	64.8	.0793	817	75.1	90.4
35	3044	3387	65.7	.0793	828	77.2	89.9
41	3044	3386	66.3	.0793	836	78.6	89.9
63	3035	3379	65.6	.0793	827	77.2	89.8

DATA SUMMARY
TABLE VI

The measurement and calibration techniques employed in testing the Resistojet in the Marquardt Electrothermal Laboratory are treated in Appendix A. The performance parameters are defined in Appendix B. Tabulated here also are the significant corrected data from the runs of 23 April and 30 April. Tables V and VI summarize the resultant important operating parameters.

A. Partial Power Performance

Partial power performance data were gathered at constant mass flow while increasing the Resistojet power to the rated conditions. The cold flow performance data are useful since they show the unique emergency thrust capability when electric power is not available. At typical spacecraft temperatures (30°C) and at rated thrustor chamber pressure, near rated thrust is produced at a specific impulse of approximately 270 seconds.

Table VII.- Emergency Capability Compared With Design

	Emergency	Design (Reference)
Gas Temperature, °K	300	2,417
Chamber pressure, atm.	8.79	8.79
Vacuum specific impulse, sec.	270	838
Mass flow, gm/sec.	0.19	0.0793
Thrust, gm-force	51.4	66.5

Figure 14 shows the component efficiencies measured while bringing the engine up to rated power for the 25-hour test. At near full power, the overall efficiency was found to be greater than expected, e.g., $\sim 77\%$, as compared to $\sim 67\%$ predicted at 825 seconds. In order to set the specific impulse $\sim I_{sp} = 825$ seconds at $P_e = 3000$ watts for the 25-hour test, the propellant flow had to be increased from 0.0748 to 0.0793 gm/sec.

Note that the pressure ratio (figure 14) across the nozzle ($A/A^* = 191:1$) was inadequate to completely expand the flow at lower power, e.g., $PR_N < 9,500$. The thrustor chamber pressure increases and hence the nozzle pressure increases with power. Thus, nozzle efficiency increases with power, dropping only as dissociation losses begin. The 30 kw Resistojet developed for the Air Force[(1)], however, shows the nozzle characteristic to be flat. See figure 15. In this case the PR_N equalled 24,000:1 for a 200:1 geometric area ratio.

(1) Contract AF33(657)-9397

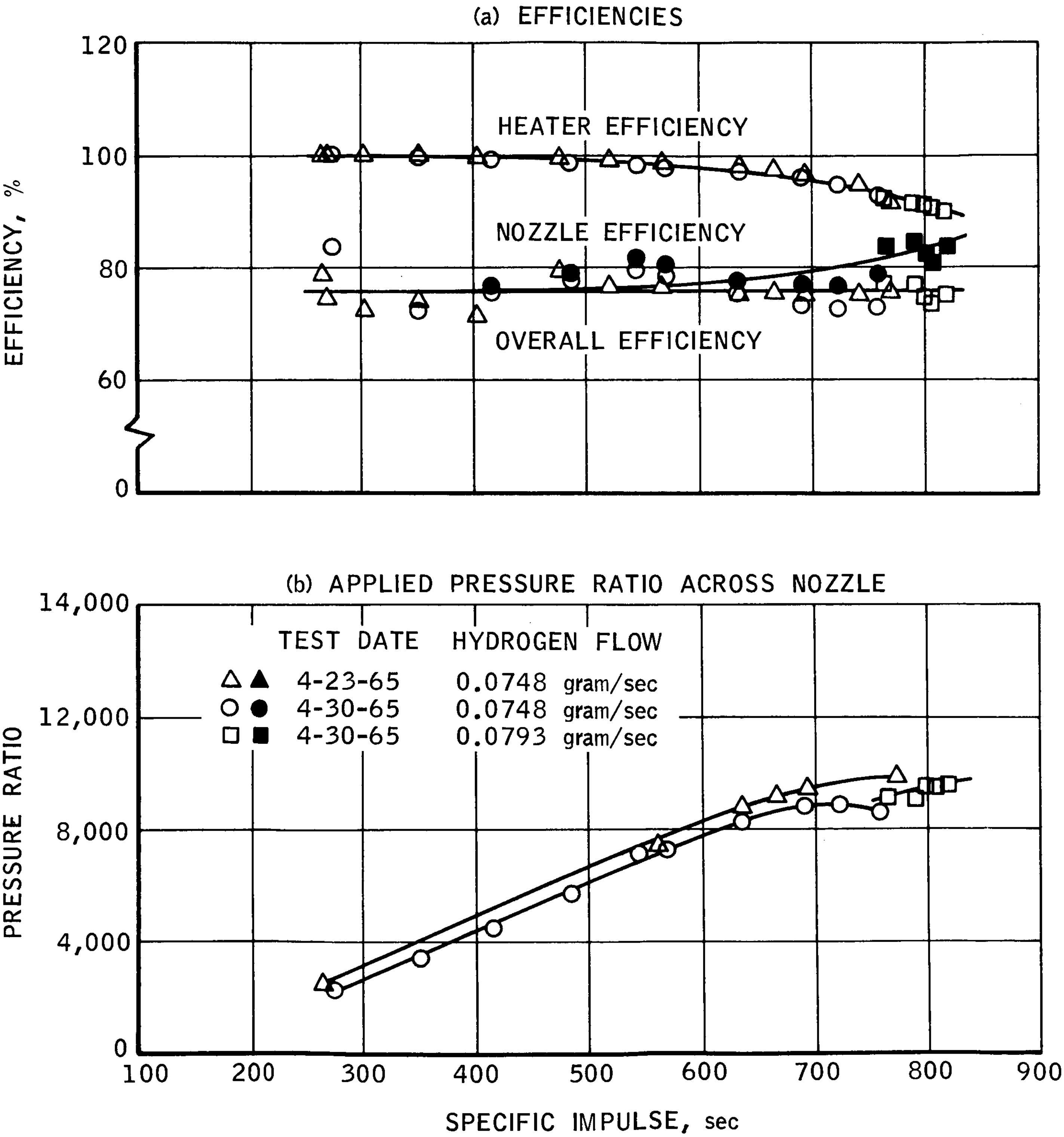

PARTIAL POWER PERFORMANCE

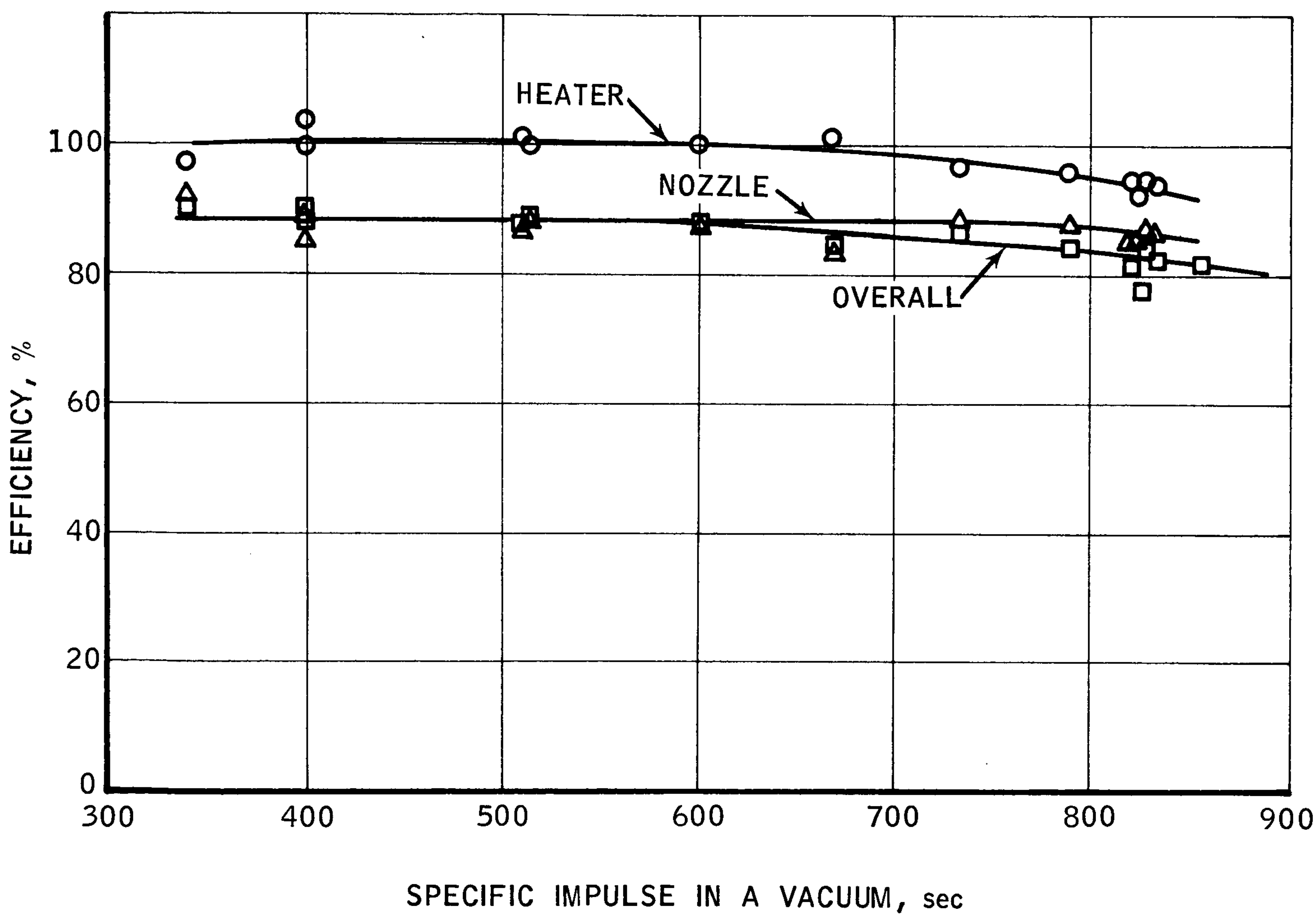

COMPONENT EFFICIENCIES, 30 KW RESISTOJET

B. Twenty-five Hour Test

On 1 May 1965, the thrustor began operation for a period of 25 hours at a power level of approximately 3000 watts and a specific impulse greater than 800 seconds. The most important performance parameters measured during the test are shown in figures 16 and 17. Data Point 35 (10.38 hours) was selected as a representative for analysis because of the particular steady conditions preceding it. The data shown in table VIII are based upon this point. The component efficiencies are compared with the 30 kw Resistojet(1) operating at reduced power but at the same vacuum specific impulse.

Table VIII.- Efficiency Comparison

Power level, P_e	3 kw	16 kw(1)
Specific impulse, $I_{sp(vac)}$	838	838
Overall efficiency, η_o	0.791	0.820
Heater efficiency, η_H	0.899	0.950
Nozzle efficiency, η_N	0.877	0.863
$A/A^*_{geom.}$	191	200

The significant point is that the nozzle performance is similar. The viscous nozzle losses previously anticipated from extrapolation of the Tinling data (ref. 15), did not materialize in the performance range here. The principal difference in overall performance is caused by heat exchanger efficiency. As units become smaller, they suffer a greater heat exchanger loss penalty.

1. Heat Exchanger Efficiency.- The heat exchanger efficiency is defined as the ratio of the power delivered to the nozzle entrance to the total supplied to the heat exchanger. Previously, heat exchanger performance was evaluated by means of an energy balance employing an exhaust calorimeter. An equivalent but more accurate method was found in evaluating the heat leaving the thrustor envelope by means of a temperature survey (see figure 13).

(1) Contract AF33(657)-9397

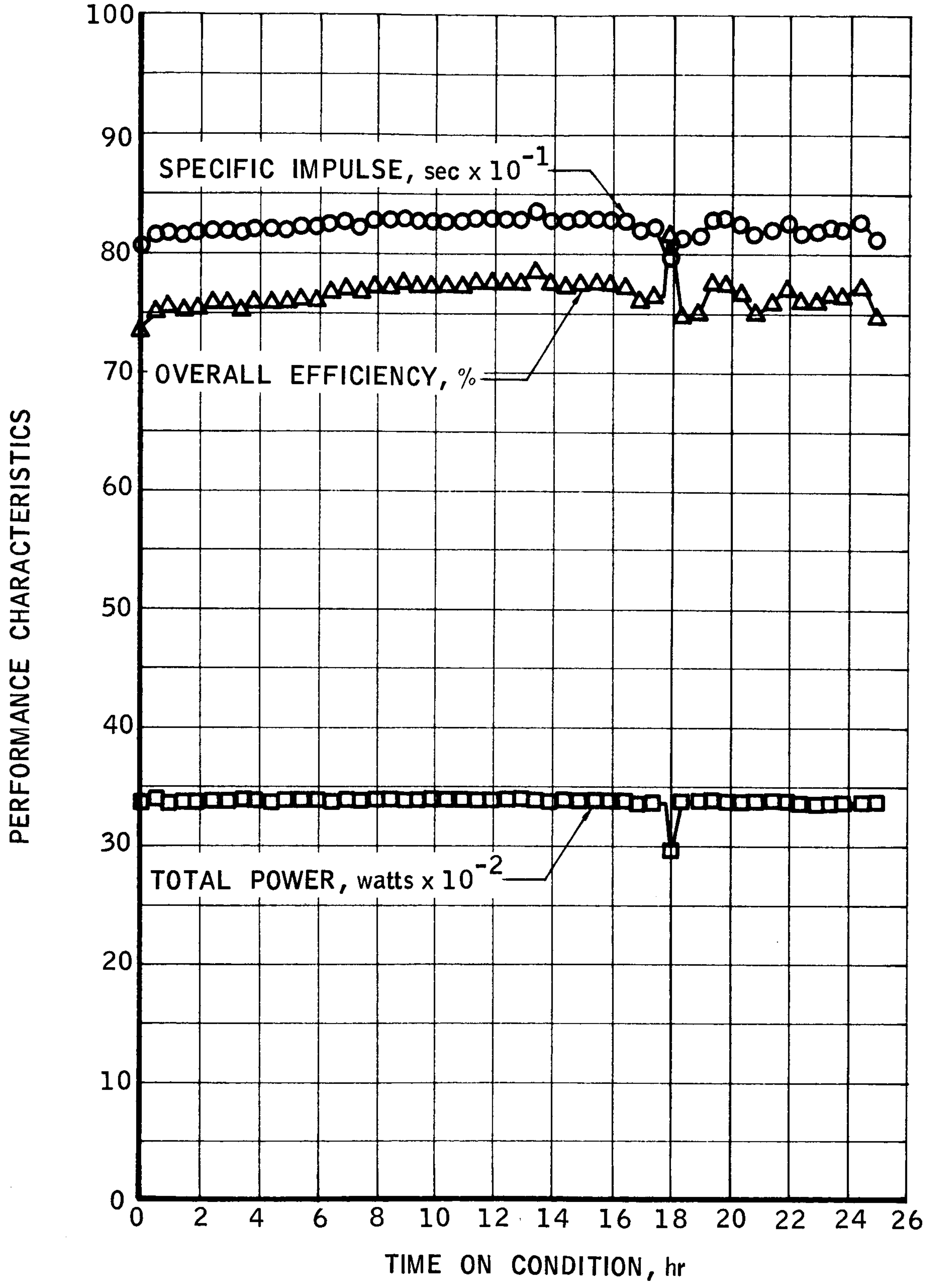

DATA SUMMARY 25 HOUR PERFORMANCE TEST

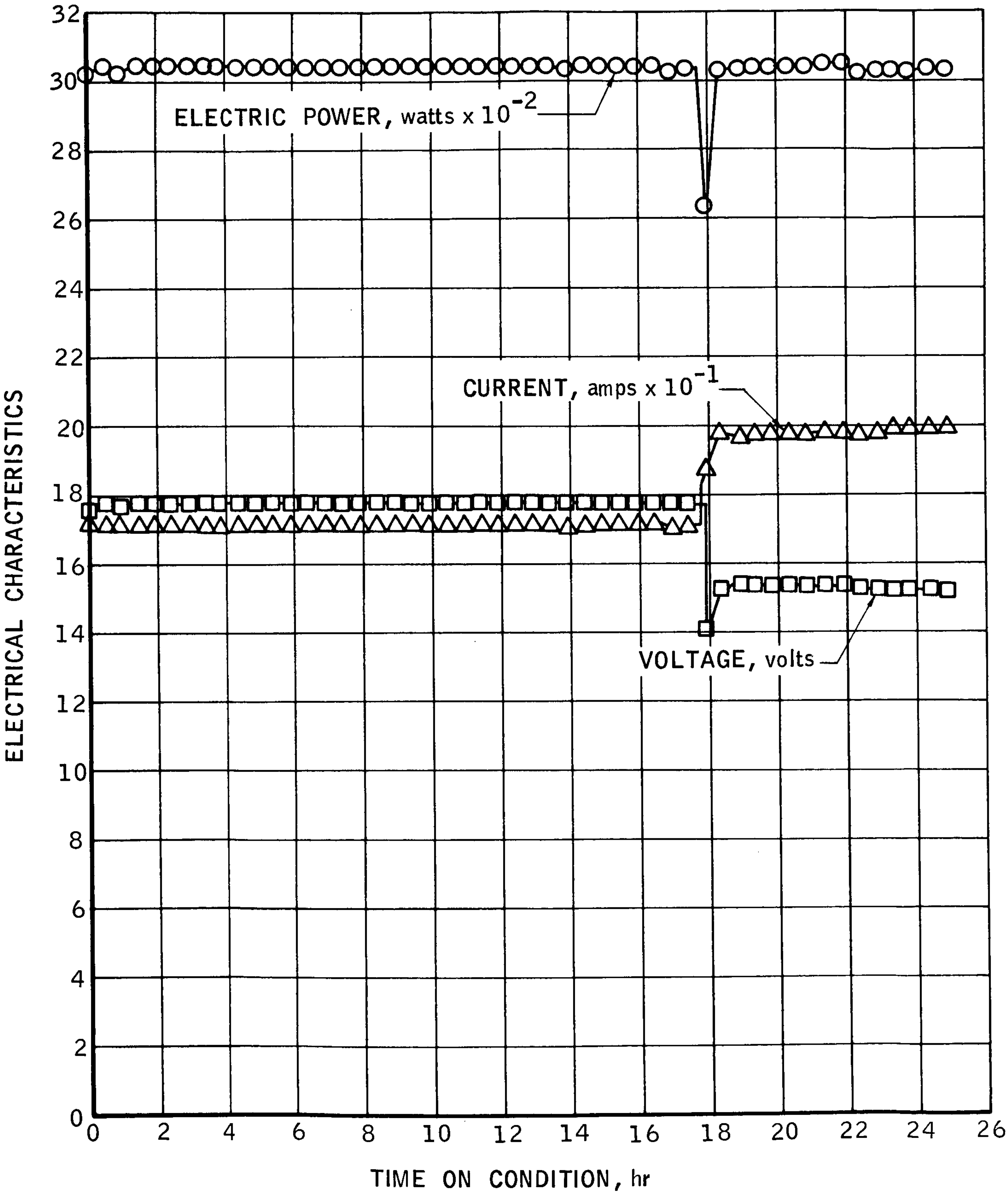

DATA SUMMARY 25 HOUR PERFORMANCE TEST

Figure 17

Table IX.- Heat Losses at 0.7 mm-Hg Ambient Pressure

	Watts
Radiation from forward thrust alignment sting access hole	3
Radiation from stainless-steel shell	310
Radiation from nozzle	4
Conduction	26
Convection	negligible

$$\eta_H = 3044/3387 = 0.899$$

With insulation replaced in the access hole and seal areas, the heat exchanger efficiency would be 0.936. With replacement of this insulation and incorporation of the higher temperature seals, the maximum surface temperature in the rear and circumferential surfaces is less than 250°C. This is an important consideration for spacecraft designers.

The radiative properties of the 321 stainless-steel shell, namely, normal total emittance, were taken from reference 22. As a check, the heat transfer through the insulation to the shell was also calculated, and the losses were found to agree with those above within 5%.

2. Nozzle Performance.- One of the unexpected experimental results was that the nozzle efficiency of the 3.0 kw Resistojet was the same as that measured on the geometrically similar 30 kw engine at the same specific impulse, 828 seconds, namely, ~ 86%.

Based on the meager data available on frictional losses due to low Reynolds numbers effects on small nozzles, a nozzle performance of 75% was predicted. The over-estimation of frictional losses compounded the calculated overall loss since a higher temperature was then estimated for the given specific impulse and this in turn caused additional estimated frozen flow losses.

The efficiency data shown in figure 14 for partial power are not significant because of the inadequate pressure ratio across the nozzle at reduced power. At design conditions, the applied nozzle pressure ratio was 9,530:1. The maximum pressure ratio required for a geometric area ratio of 191:1 under frozen flow conditions is 9,500:1. Therefore, at design the nozzle was completely filled with supersonic flow.

3. Throat Stability.- The throat diameter was initially measured to be 0.75 ± 0.013 mm. At the conclusion of the 25-hour test, it was carefully measured and found to be 0.747 ± 0.003 mm.

Experience with earlier high-pressure Resistojets found the throat diameter to close 8% in 35.6 hours. This was brought about by the vapor-deposition of the sublimed tungsten at the throat. This can be detected by a change in chamber pressure for the same power and mass flow. The average supply pressure climbed slightly (0.8%). The redundant pressure measurement, using a precision Heise gauge, showed no such increase but only a fluctuation of $\pm$ 0.5%. This indicates that the throat diameter is stable for these conditions.

The temperature measurement of the inner element and throat was attempted. See Appendix A. A temperature of 2120°K is reported by the pyrometer and is believed close to nozzle wall temperature at the throat.

4. Electrical.- The steady-state thrustor resistance as a function of gas temperature is shown in figure 18. This shows the ratio of hot resistance to cold ($I_{sp} = 828$) to be $\sim 7.5:1$. This is not an unfortunate characteristic with regard to direct connection to solar cells. Solar cells tend towards a constant-current limit, hence the operating point during starting is current-limited until the design voltage is reached. The power may thus be progressively applied without additional controls providing the solar cell characteristic is so utilized.

5. Seals.- The cold flow leakage prior to the 25-hour test was of the order of 10^{-5} gm/sec, a negligible quantity. During the course of the test as is shown in figure 19, the seal temperature rose to 790°C. The Inconel-X silver-plated static seals performed in excess of their design ratings with no difficulty encountered. No increase in leakage was experienced as a result of the 25-hour test plus 12 hours of partial-power performance testing. In order to provide a margin of safety, gold-plated René 41 seals were ordered. These did not arrive in time for the 25-hour test, but were installed in the engine before shipment to the Lewis Research Center.

6. Heat Exchanger Elements.- The tungsten vapor-deposited heat exchanger elements performed outstandingly. No elements were destroyed in testing or handling before or subsequent to the test. The one instance of a crack occurred in the flared support area of the -15 element before testing. This was treated by drilling a 0.2 mm stop hole. See figure 20, bottom left. The element was successfully used in all testing.

The heat exchanger used in the test was reinstalled for shipment to the Lewis Research Center.

7. Tungsten Sublimation.- The exchanger elements experienced only a small weight change in the testing program. It is not certain whether this represents sublimation or reduction of surface impurities. Because of element bonding, the first six elements had to be weighed as a set. Initially, the elements were weighed in assembled pairs.

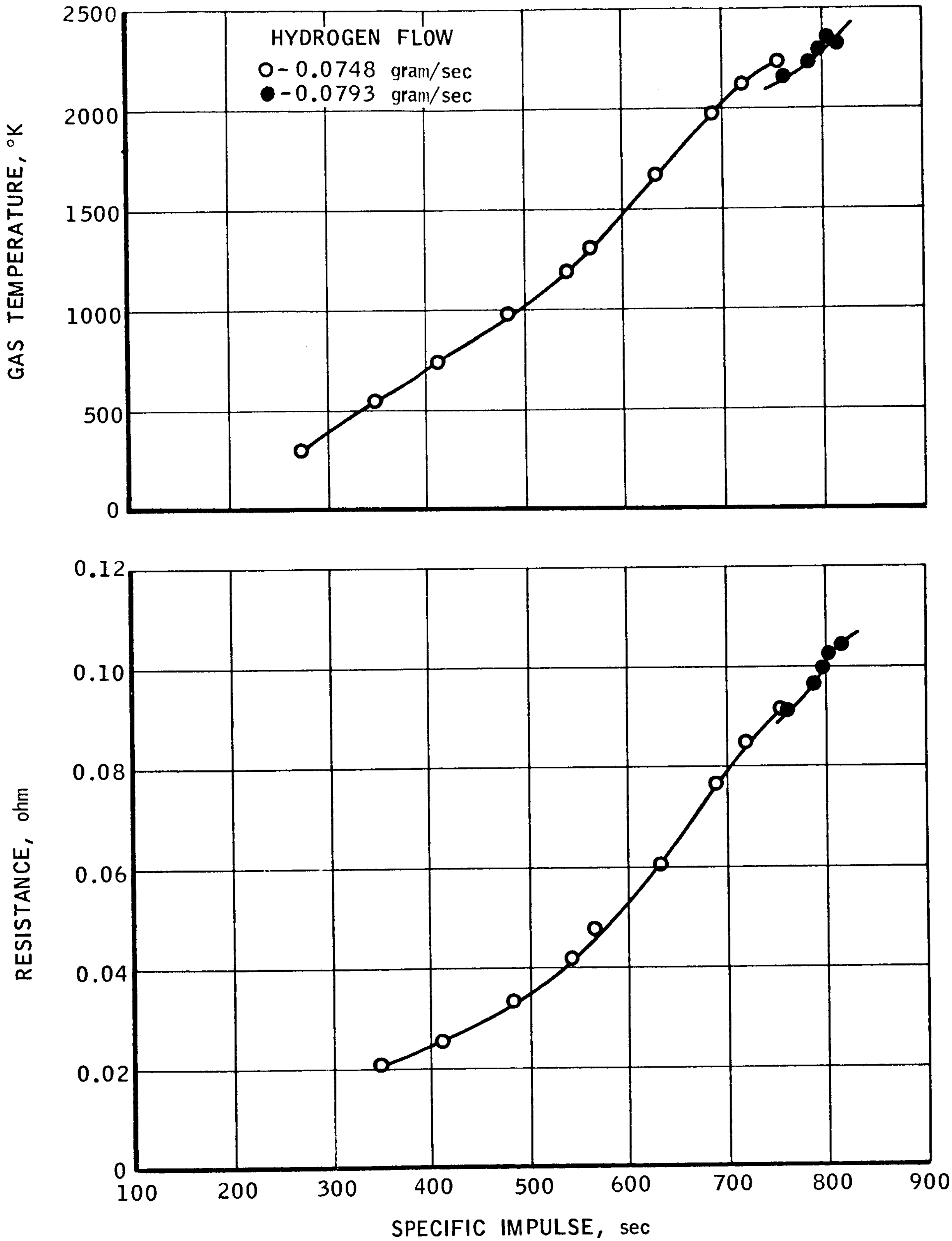

THRUSTOR RESISTANCE AT PARTIAL POWER OF 3 KW RESISTOJET

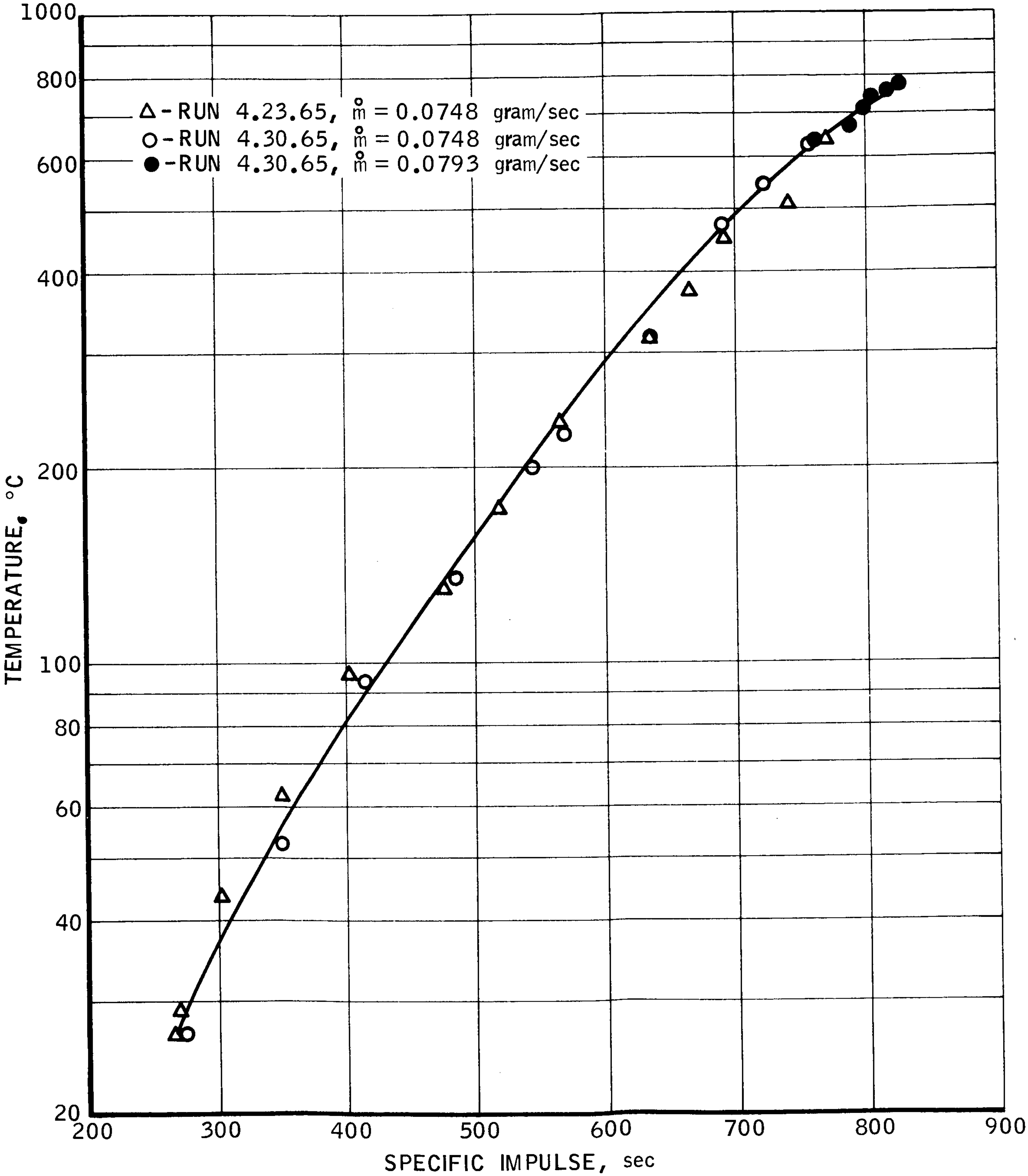

CASE SEAL AREA TEMPERATURE

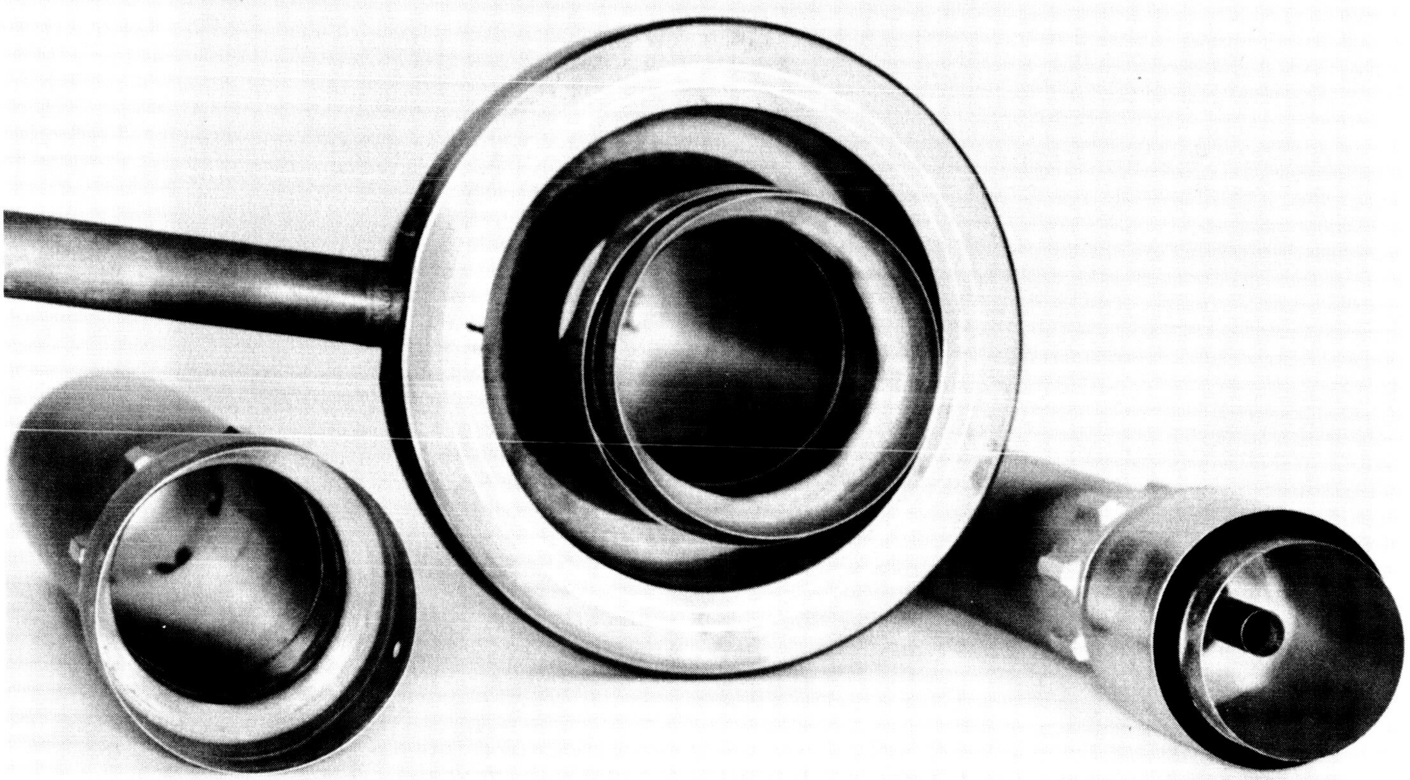

TUNGSTEN HEAT EXCHANGER AND SHIELDS
AFTER 25 HOUR TEST

Table X.- Heat Exchanger Weight Loss

Elements (see table II)	Weight, grams Before	After
-3, -5, -7, -9, -11, -13 (inner)	82.5	82.0
-15, -17	44.9	44.8

This weight reduction represented the loss due to total testing of the unit, or 25 hours above 800 seconds, 4 hours above and 22 hours below 700 seconds. According to the sublimation bench tests of Howard and Short (ref. 23), the loss for the first six elements would be negligible due to the relatively low element temperatures. The measured loss is probably due to the removal of impurities from the tube surfaces. Because of the small differences in heat exchanger weight over the test, it is possible to predict life greatly in excess of 25 hours.

8. Stabilized Resistance.- A comparison of the calculated heat exchanger resistance with that actually measured before and after bonding is summarized in table XI.

Table XI.- Heat Exchanger Resistance

Specific Impulse (sec)	Gas Temperature (°K)	Resistance ohms Calculated	Measured Before Bonding	Measured After Bonding
270	300	0.0090	0.0143	--
828	2400	0.080	0.1041	0.0778

The calculated cold resistance (excluding contact resistance) for the actual heat exchanger, the physical characteristics of which are summarized in table II, is 0.00901 ohms. The actual resistance, however, was 0.0143 ohms measured by a precision impedance bridge. The difference was the contact resistance at the element joints.

When power was applied to the engine, the resistance increased due to the increase in resistivity with temperature and the increase in contact resistance with contact voltage. As the engine was taken up in power, at first the current increased more rapidly than the voltage. As the temperature rose and the resistance increased, the current stabilized. See figure 21 for the equilibrium partial-power performance. After approximately 17.4 hours at a specific impulse above 800 seconds, a voltage of 17.8 volts, and a current of 171 amps, the bonding process suddenly accelerated and joined most of the tubes. At this

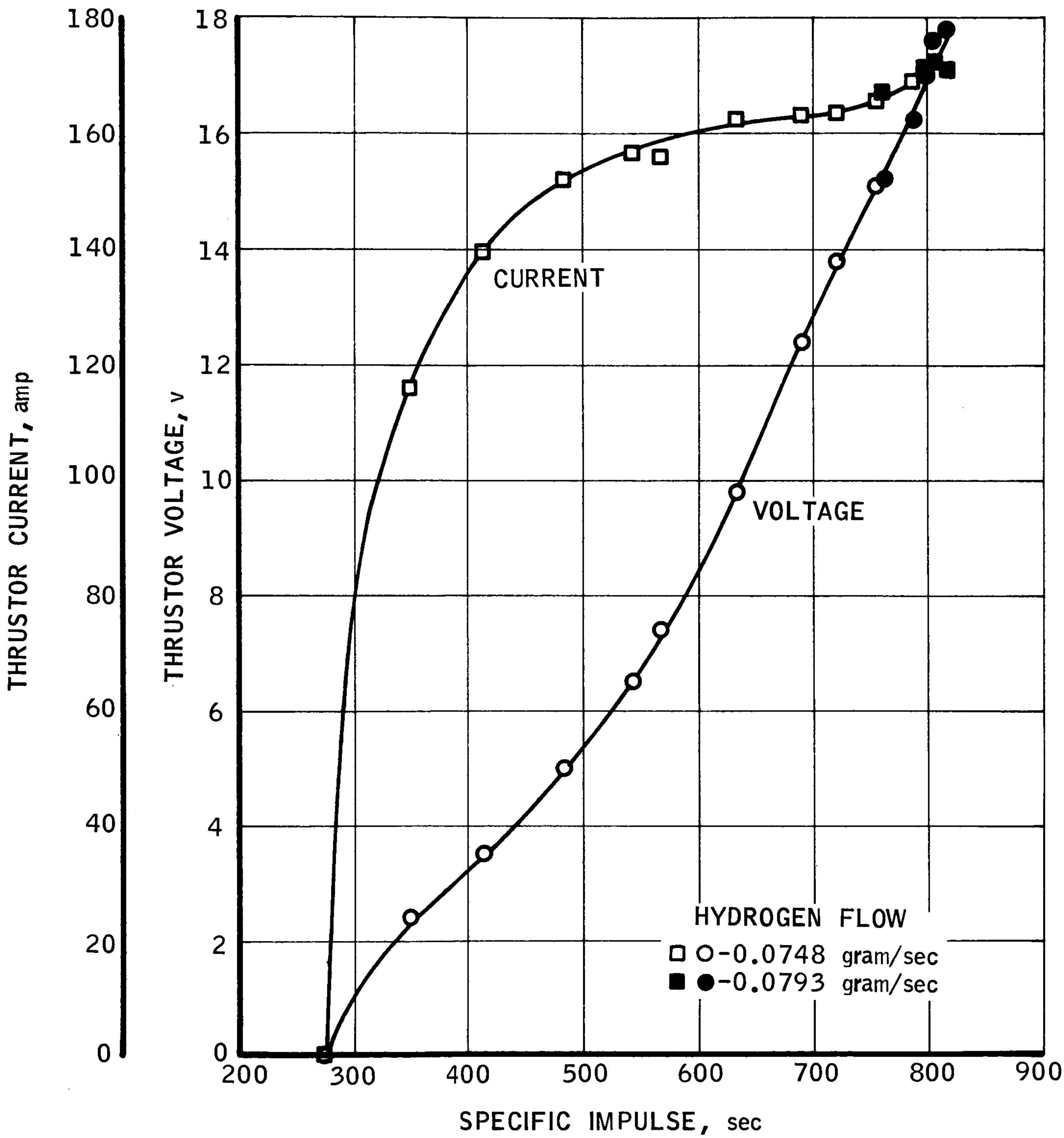

PARTIAL POWER ELECTRICAL CHARACTERISTICS OF 3 KW RESISTOJET point, the hot resistance of the engine dropped from 0.1041 to 0.0778 ohms, causing a corresponding change in voltage and current for the same power level, figure 17. Using a calculated temperature distribution, the original calculated cold resistance of 0.0090 ohms increased to a hot resistance of approximately 0.08 ohms, assuming no contact resistance. This comparison indicates that the contact resistance disappeared.

C. Increased Performance Potential

While the specific impulse and efficiency exceeded its contractual goals, the maximum performance potential could not be demonstrated during this period. It is recommended that this be done after life-verification at the Lewis Research Center.

With the René 41 seals (Section III.E), seal temperature capability of 926°C is possible. From figure 19, a specific impulse capability of 890 seconds is then indicated. An overall efficiency of 0.70 is conservatively projected based on the experimental results presented here. At an electric power of 3.0 kw and a mass flow of 0.06 gm/sec, a thrust of 53.4 gms force would result at thrustor chamber conditions of 2720°K and 7.14 atmospheres. This is the same chamber temperature as originally planned to meet the performance objective. A long engine life is expected.

SEAL AREA AFTER 25 HOUR TEST

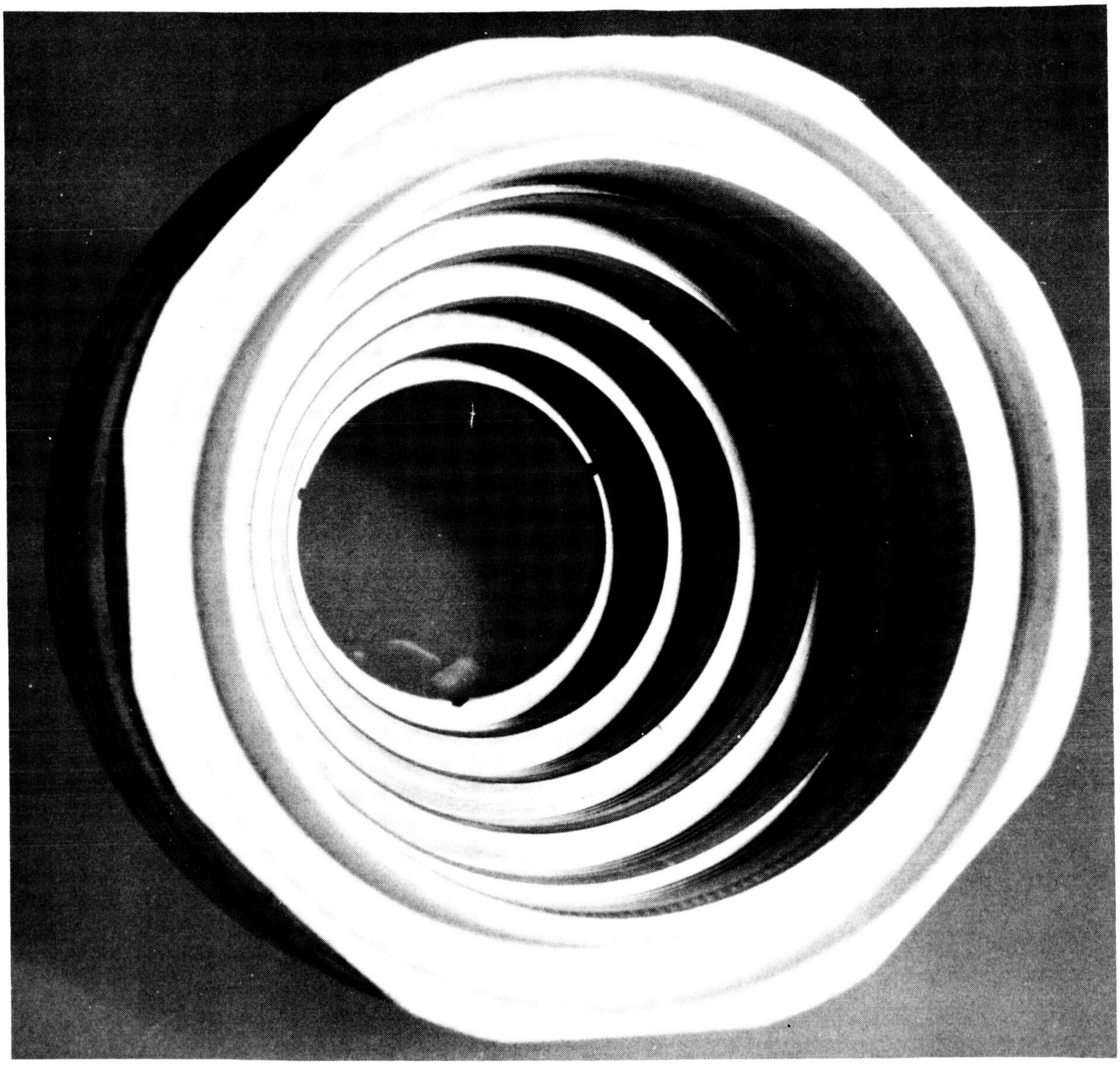

BORON NITRIDE HEAT EXCHANGER SUPPORT

AFTER 25 HOUR TEST

VI. CONCLUSIONS & RECOMMENDATIONS

1. The heat transfer analysis and experimental results show that the concentric tube heat exchanger concept requires only a small wall over-temperature of about 60°C above the needed gas temperature. The resultant low tungsten sublimation rates allow a longer life potential than other designs.

2. On the basis of the successful 25-hour performance test, it is recommended that the delivered engine be tested to demonstrate:

   a. extended life (~ 1000 hours)
   b. higher specific impulse capability

References

1. Douglas Aircraft Co., Inc., Missile and Space Systems Division, "Report On A System Comparison and Selection Study of A Manned Orbital Research Laboratory". NASA Contract NAS 1-2974, SM 44592, Vol. I, Sept. 1963, 96.

2. Jack, John R., "Theoretical Performance of Propellants Suitable for Electrothermal Jet Engines." 15th Annual Meeting, ARS, Washington, D.C., December 1960, ARS Preprint No. 1506-60; later published ARS J 31, 1685-1689 (1961).

3. Howard, James M., "The Resistojet". ARS Space Flight Report To The Nation, ARS Preprint 61-2126 (October 1961); also ARS J 32, No. 6, 961-962, June 1962.

4. Howard, James M., "Investigation of Electric Resistance-Heated Rocket For Feasibility In Space Propulsion Applications". ASD TDR-62-487, June 1962.

5. Jack, John R., "NASA Research on Resistance Heated Hydrogen Jets". AFOSR Third Symposium on Advanced Propulsion Concepts, Cincinnati, Ohio, October 2, 3, 4, 1962.

6. Page, Russell J., and Halbach, Carl R., "Resistojet Engine Performance - A Comparison of Experiment with Theory". Presented at the AIAA 4th Electric Propulsion Conference, Philadelphia, Pa., August 31, 1964.

7. Todd, James P., "Resistance-Heated Thrustor Research". Plasmadyne Report ITR 093-19628, September 1963.

8. Bennett, Stewart, "Electrothermal Engine Research and Development". Report NASA CR-54104.

9. John, Richard R., and Morgan, Dean, "Resistojet Research and Development - Phase II". Second Quarterly Progress Report, NASA CR-54333, January 20, 1965.

10. Oswalt, L. R., and Widawsky, Arthur, "Investigation of Exhaust Nozzle Flow Phenomena in Arc Jet Engines". Contract NAS 8-8951, 31 May 1962.

11. Spisz, E. W., "Compilation of Theoretical Rocket Performance for the Chemically Frozen Expansion of Hydrogen". NASA TN D-2080, December 1963.

12. Sutton, G. P., "Elements of Rocket Propulsion". First Edition, John Wiley & Sons, 1949.

13. Pitkin, E., "Optimization of Conical Nozzle Angle With Viscous Velocity Profile". The Marquardt Corporation, December 13, 1962.

14. Pitkin, E. T., "Viscous Laminar Flow in Conical Nozzles". MR-20,187, The Marquardt Corporation, July 1962.

15. Tinling, B. E., "Measured Steady-State Performance of Water Vapor Jets For Use In Space Attitude Control Systems". NASA TN D-1302, May 1962.

16. Simmons, F. S., "Analytic Determination of the Discharge Coefficients of Flow Nozzles". NACA TN 3447, Washington, D.C., April 1955.

17. Page, Russell J., "A Final Report On The Development Of The 30 KW Resistojet Engine Including Results of Extended High Temperature Life Tests". MR-20,333, June 1965.

18. Mills, R. G., Lindgren, J. R., and Weinberg, A. F., "An Evaluation of Vapor-Deposited Tungsten Tubing". NASA CR-54277, GA-5721, General Atomic Div. of General Dynamics, October 19, 1964.

19. Direct Conversion Project Staff, "Vapor-Deposited Tungsten". NASA Contract NAS3-4165, NASA CR-54266, GA-5640, General Atomic Division of General Dynamics, October 9, 1964.

20. Holm, Ragnar, and Holm, Else, "Electric Contacts Handbook." Third Edition, Springer-Verlag, Berlin, 1958.

21. Albom, M. J., "Joining Tungsten To Tungsten". Materials & Design Engineering, June 1962.

22. Wood, W. D., Deem, H. W., and Lucks, C. F., "Thermal Radiative Properties of Selected Materials". Report to Office of Director of Defense Research and Engineering, Defense Metals Information Center, Battelle Memorial Institute, Columbus, Ohio; Report 177, Vol. 1, 65, November 15, 1962.

23. Short, G. R., and Howard, J. M., "Sublimation of Tungsten in Hydrogen". ARS Preprint, March 1963.

24. Stoner, Willis, Sinlette, John T., Jr., DeViney, Wm., "Thrust Dynamometer and Calorimeter for a Thermoelectric Thrustor". Thrust Systems Corporation Final Report TR-1 to The Marquardt Corporation, April 1963.

25. Stoner, Willis, "Performance Analysis of The Model 102 Thrust Dynamometer and The Model 193 Exhaust Calorimeter". Report TR-2 to The Marquardt Corporation, July 1963.

26. King, C. R., "Compilation of Thermodynamic Properties, Transport Properties, and Theoretical Rocket Performance of Gaseous Hydrogen". NASA TN D-275, April 1960.

27. Page, Russell J., et al, "Arc Plasma Thrustor Studies". 15th Annual Meeting, ARS, Washington, D.C., ARS Preprint No. 1505-60, December 1960.

APPENDIX A

1. Laboratory Description

The interior of the Electrothermal Laboratory is shown in figure 24. The vacuum cell, 1.2 meters in diameter, 2 meters long, is mounted on rollers for easy access. The thrust dynamometer is mounted on the stationary forward cell end. Pyrex windows are located on each side with a rear window for pyrometric measurements. The vacuum-pumping system is connected to the cell through an exhaust gas calorimeter.

Both the rectifier and hydrogen tank bottle farm are located adjacent to the laboratory.

A. Vacuum System.- To simulate suitable vacuum conditions, the laboratory includes a main vacuum-pumping station adjacent to the laboratory building and connected through a vacuum line to the research thrust chamber. The vacuum pipeline contains specially selected bellows-type flexible connections and the environmental chamber utilizes a seismic mass as a base.

A three-stage vacuum system is used. The first stage consists of a Roots-Connersville 4342 liters-per-second (9200cfm) positive-displacement lobe-type, rotary pump, modified to handle hydrogen gas at low pressures. A water-cooled heat exchanger at the inlet port of the first stage reduces gas temperatures, thus maintaining the efficiency of the booster. The second, or intermediate stage, consists of two Stokes 615 liters-per-second (1300 cfm) positive-displacement lobe-type, rotary pumps connected in parallel through a manifold and heat exchanger to the outlet of the first stage booster, and maintaining a pressure ratio of 5:1. The third, or last stage, unit consists of two 142 liters-per-second (300 cfm) mechanical pumps, each on a separate manifold to its intermediate booster.

The system is capable of evacuating a closed vacuum chamber with a volumetric displacement of at least 7080 liters from atmospheric pressure (760 mm-Hg to 10^{-2} millimeters of mercury at ambient temperatures within a time limit equal to or less than seven minutes.

The system will effectively handle between 4320 and 4720 liters per second of hydrogen gas at pressures of 1.0 to 1.5 millimeter of mercury in the chamber. This constitutes hydrogen propellant flows of 0.4536 grams per second. These capabilities are based on gas temperature of 37°C; the gas has been cooled down by heat exchangers in the system. With no-flow conditions, the vacuum system will, over a period of time, blank out approximately at 0.5 microns of mercury.

The steady pumping capabilities of the system as a function of pressure are shown in figure 25 for hydrogen, ammonia, and argon.

B. Power Supplies.- The power supplies used consist of one unit rated at 50 kilowatts with control for 0 to 735 amperes at 0 to 75 volts D.C., and 0 to 1100 amperes at 0 to 50 volts D.C.

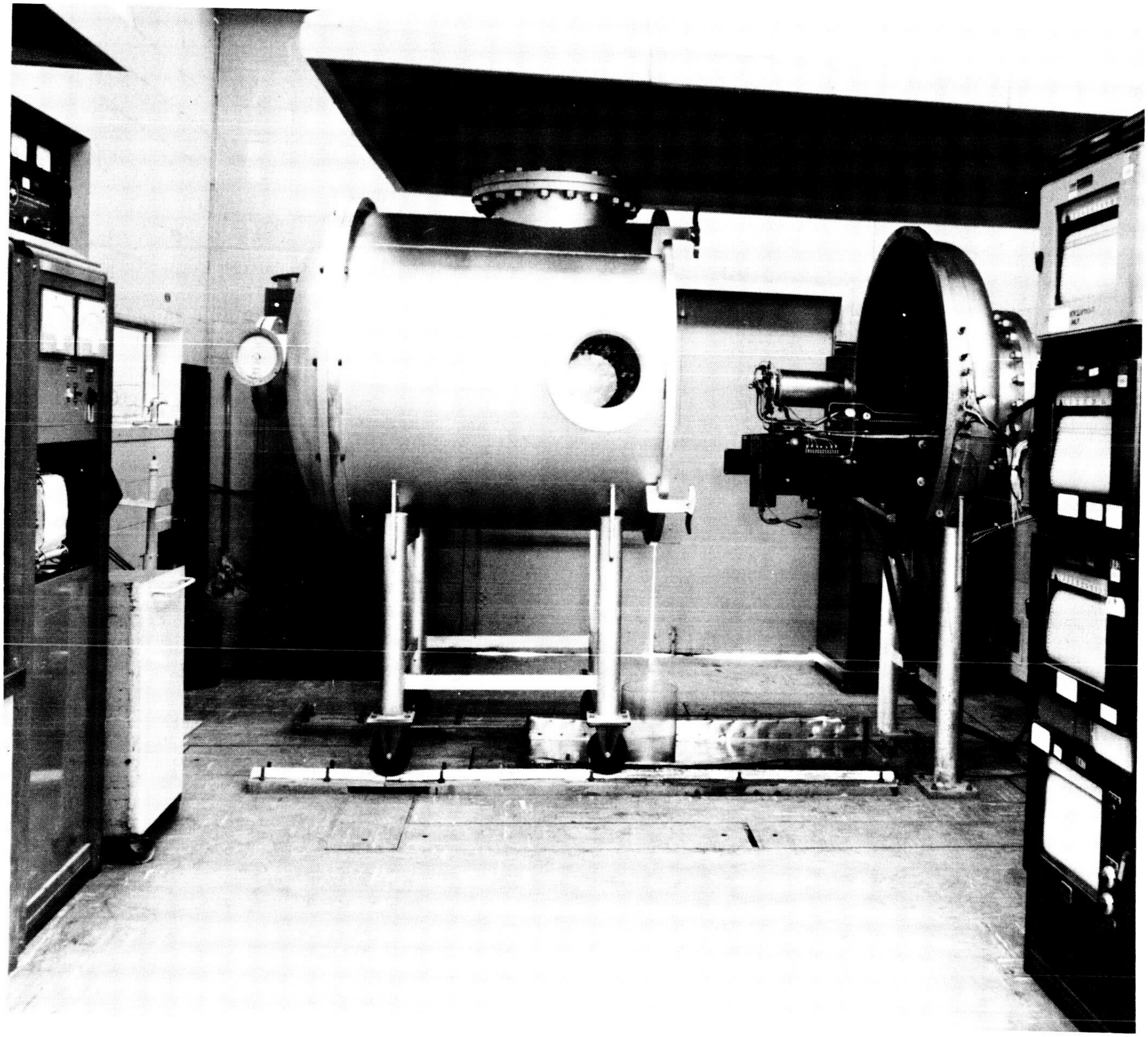

ASTRO ELECTROTHERMAL PROPULSION LABORATORY

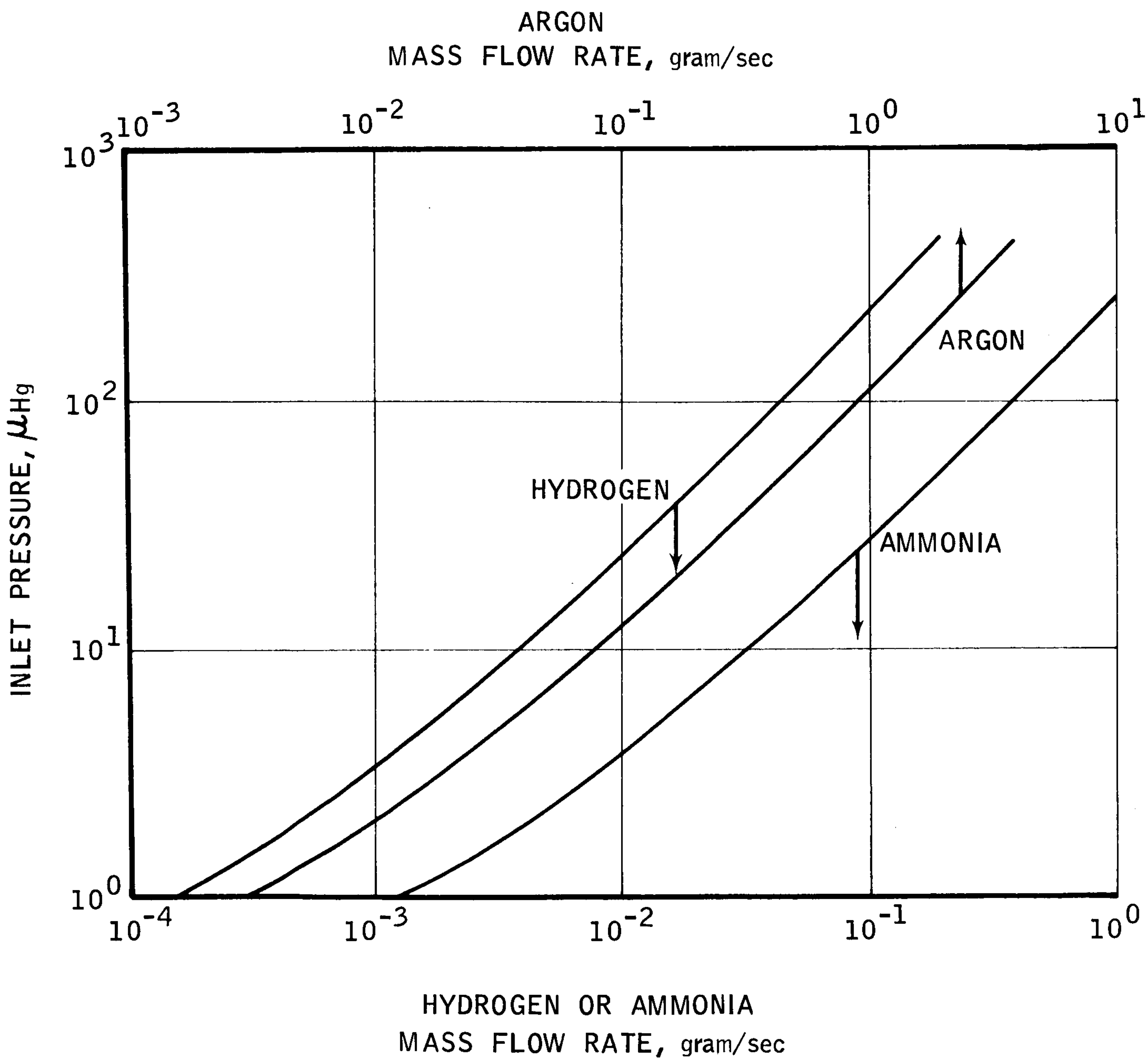

INLET PRESSURE OF AN 18 X 41 HIGH VACUUM ROOTS BLOWER AS A FUNCTION OF MASS FLOW RATE

2. Thrust Measurement

It is important to recall that the basic objective is to determine in an earth-bound laboratory the net thrust that would be produced by an electric thrustor in free space. "Apparent" thrusts can be introduced into electrical propulsion thrust measurements from a number of effects if great care is not exercised. Extraneous forces can cause errors due to gravitational, inertial, aerodynamic, elastic, thermoelastic and electromagnetic effects. Dimensional and angular errors from thermal, elastic effects, not to mention carelessness, can cause similar inaccuracies.

For the above reasons, an independent study was made of dynamometer systems and is reported in reference 24. As a result, a new type of thrust dynamometer was designed for the Resistojet program to minimize these errors.

Figure 26 is a sectioned isometric drawing of the dynamometer, illustrating its principles. The unique feature is the fact that the thrustor suspension floats. The primary advantages are: 1) the elimination of any gravity-induced restoring force such as that encountered with the simple hanging pendulum, and, 2) the critical lengths of moment arms are easily maintained at uniform temperature by submergence in cooled vacuum oil (Dow Corning DC-704) without the possibility of apparent thrusts caused by otherwise integral cooling loops.

Figure 27 shows the pivoted radial beam, mounted horizontally with the suspension primarily supported by two floats in mercury pools. The vertical pivot axis, consisting of light Bendix flexure, positions the suspension and prevents tilting of the mount when thrust is applied. The resultant suspension system is not stiff and has a natural frequency of 1.67 cycles per second.

In addition, a horizontal pivot axis is provided in the radial arm to guide in adjusting the mercury level so that the weight is supported primarily by floatation. After leveling, a fitted pin ("vertical lock pin") is inserted to prevent motion of the horizontal pivot so that the same thrustor moment arm is always maintained. A Statham transducer is used to provide the thrust measurement signal. The transducer, with its case carefully perforated, is submerged in the vacuum oil to provide uniform temperature over its sensing element.

The design avoids bridging the balance with stiff electrical cables and hoses. Also, such induced forces as Bourdon-tube effects in hoses and Lorentz forces between electrical leads are avoided. Electric power is taken aboard the balance through electrodes immersed in mercury. Propellant is taken through a compact flexible array (0.25 inch stainless line) which is equivalent to the flexibility of a 12-foot long torsion tube. All electrical leads from transducers and thermocouples are taken from the balance over the pivot point.

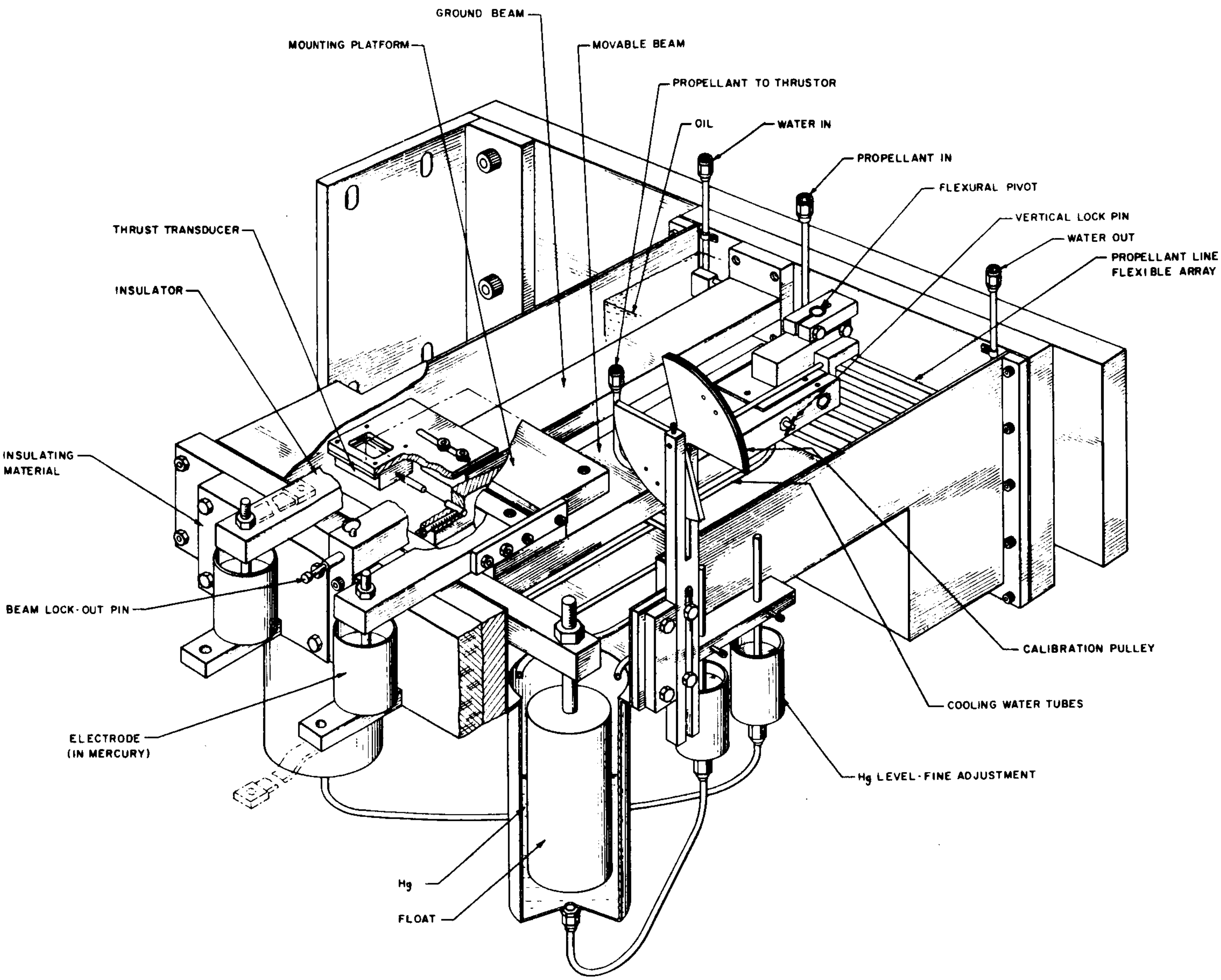

FLOATATION TYPE LOW THRUST DYNAMOMETER

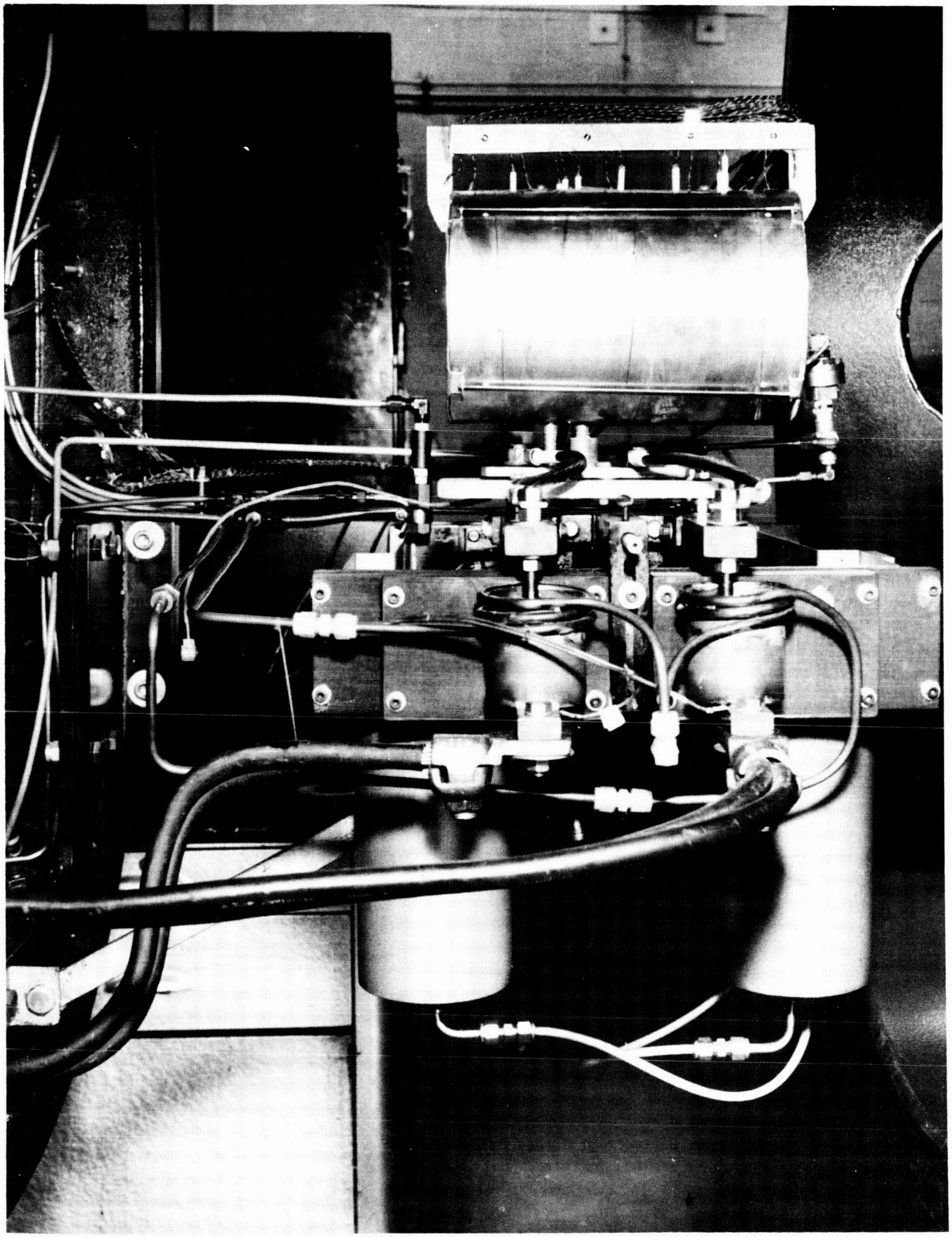

LABORATORY 3 KW RESISTOJET
INSTALLED ON THRUST DYNAMOMETER

The dynamometer system, which includes a Midwestern Oscillograph recorder, is calibrated by means of precision weights suspended over a calibration pulley employing frictionless Bendix pivots. The thrust axis of the thrustor is aligned with the top of the pulley to insure colinearity of the thrust and calibration axis, by means of a calibration sting which screws into the back of the thrustor.

Figure 28 shows the results of the calibration immediately preceding the 25-hour performance test reported. This calibration, because of a damaged pulley, used a polished teflon pin and a 0.75 pound test monofilament line. A shift at zero thrust occurred under vacuum. A "60-gram point" calibration under vacuum conditions verified using the calibration based upon the zero reference under vacuum conditions.

Thrust under space vacuum conditions may be found by adding the usual correction

$$\Delta F = (\text{nozzle exit area}) \times (\text{cell pressure}) \qquad (A.1)$$

This correction is applicable when the nozzle "runs full" under cell conditions. In the case of the 25-hour run, the additive correction to I_{sp} was small, namely 10 seconds. It was <u>not</u> included in the data presented.

A detailed performance analysis of the dynamometer (design thrust = 450 grams) was reported in reference 25. Operating under the present thrust level (65 grams) the probable error is estimated to be 2%.

3. Propellant Flow Measurement

The schematic of the flow measurement system used for all such data reported herein is shown in figure 29. The metering element was a Cox rotometer (Model 129A 0623-91). The scale, some 40 cm in length, covered a flow range of from 0.4 to 2.6 x 10^{-4} lb/sec. The measurement of flow in such meters is density-dependent, hence the hydrogen pressure and temperature were carefully regulated. A Grove hand-loader, followed by a micrometer needle control valve, maintained a pressure of 300 psia, as observed on a Heise gauge. The temperature was maintained at 30°C by passing the gas flow through a thermostatically-regulated water bath.

The Cox flowmeter was calibrated in two ways; first, by a volumetric "prover" on air and CO_2 at the same Reynolds number as at test conditions. This was done at Fisher and Porter (Anaheim, California). The second calibration was done in our laboratory on hydrogen using the buoyant force measurement technique with a meteorological balloon.

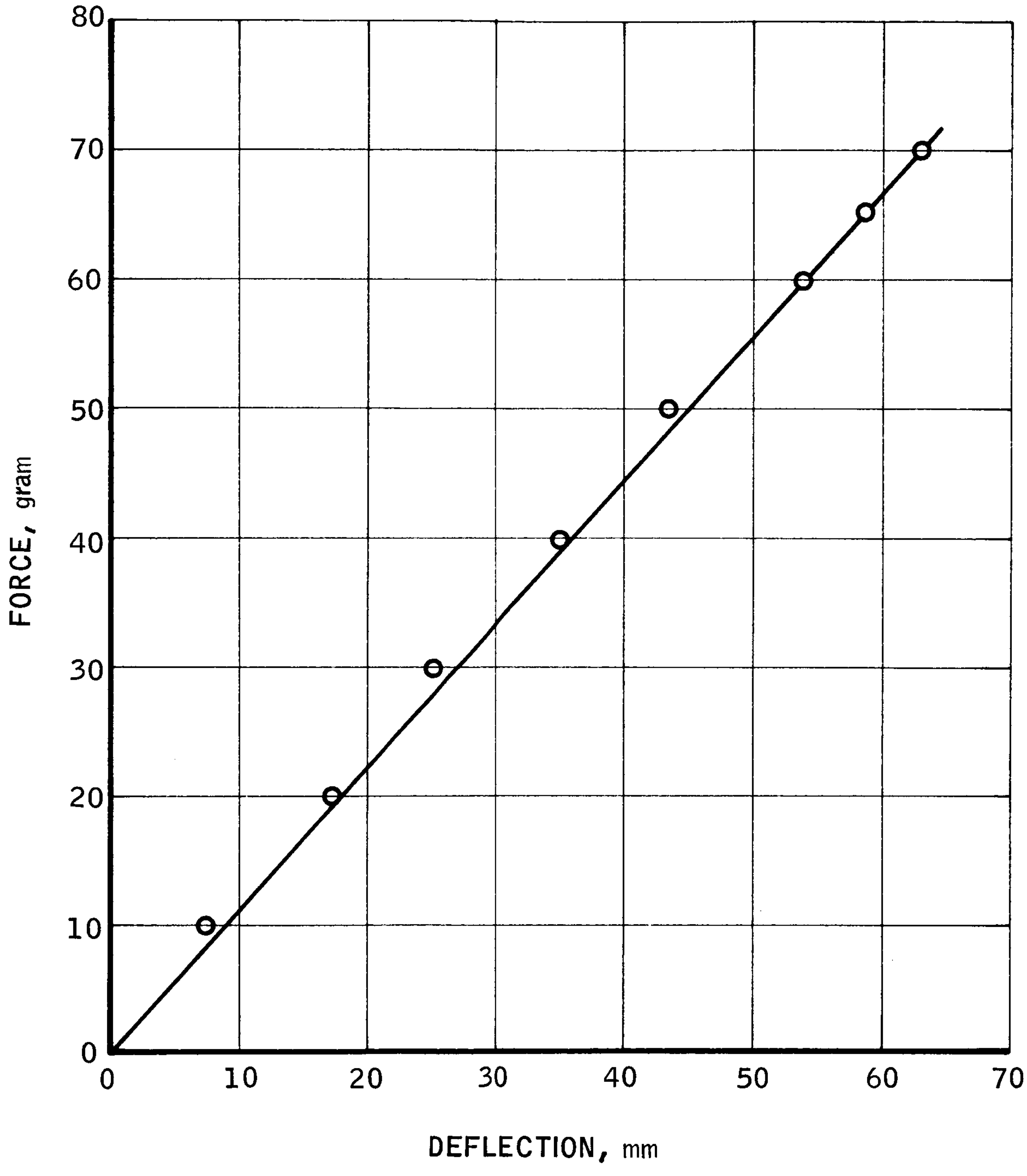

THRUST DYNAMOMETER CALIBRATION

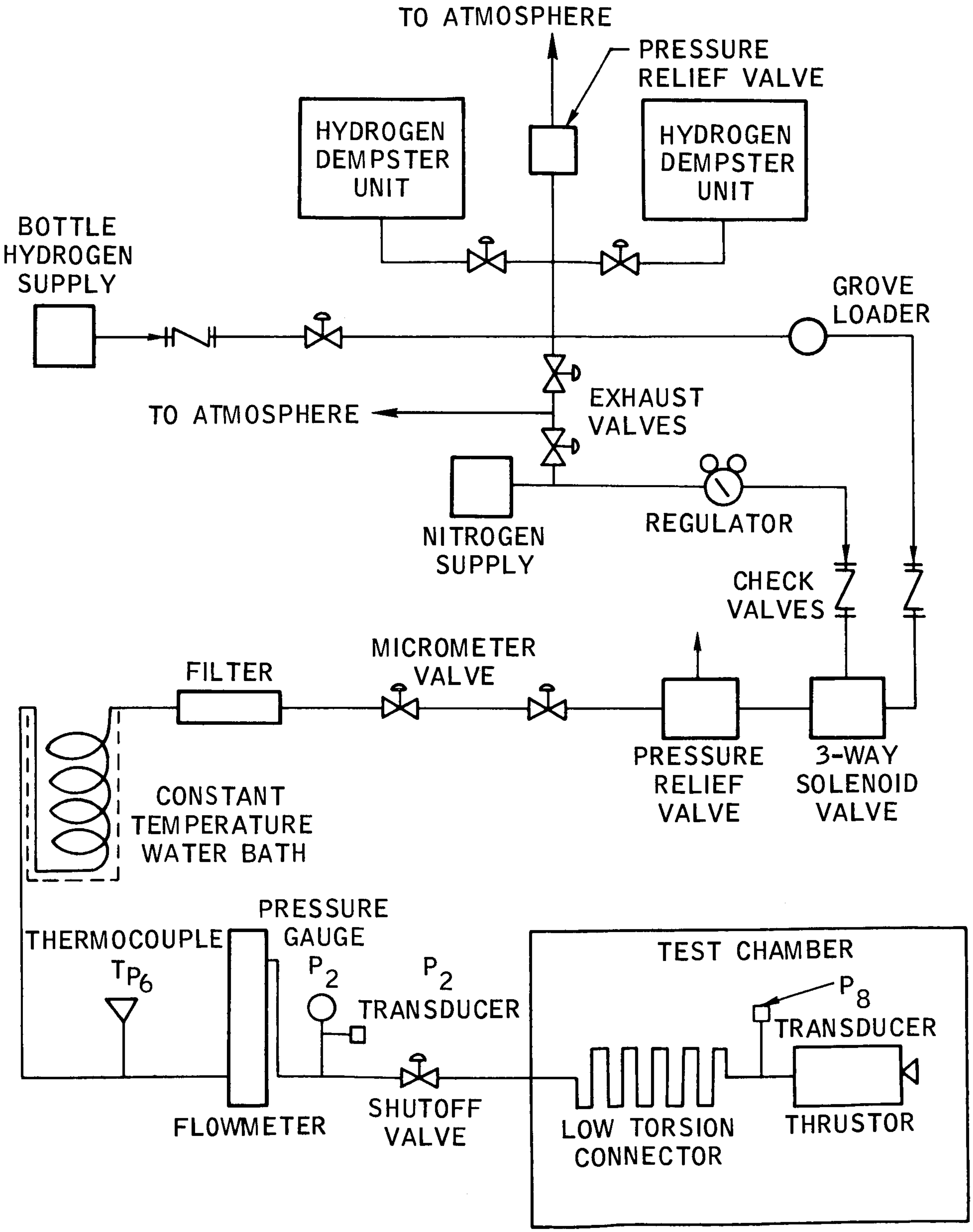

HYDROGEN FLOW DIAGRAM

Figure 29

The buoyant force method is based upon Archimedes' principle, namely, the relation between the buoyant force and the mass of the hydrogen in the meteroological balloon are related

$$F = V\left[\rho_a - \rho_h\right] \qquad (A.2)$$

where V is the volume of the hydrogen, ρ_a and ρ_h are the densities of the surrounding air and the hydrogen, respectively. The mass flow may then be found from Equation A.3,

$$\dot{m} = \frac{F}{\Delta t\left[\frac{\rho_a}{\rho_h} - 1\right]} \qquad (A.3)$$

During the flow meter calibration, the propellant was passed through the actual flow system and then diverted to the balloon at engine entrance. The precision balance upon which the balloon is held by weights is first over-balanced. Next, the flow is set and allowed to become steady. As the pointer swings through the balance point, a stop watch is started. A precision weight is added to the pan and the time measured until the balance again swings through zero. This measurement then represents the time, Δt, for the buoyant force, F, to change by the amount of the precision weight added to the pan. This measure repeated within 0.3% maximum error. The method generally assumes that the temperature and the pressure of the gases inside and outside the balloon are equal. These assumptions were checked and found not necessarily correct. The buoyancy of the balloon, at no flow, was checked for a period of 10 minutes, with negligible change indicating no leakage or thermal changes. The pressure inside the meteorological balloon relative to air was measured by a precision draft gauge and found to be 9 centimeters of water. This amounted to a correction of 1 percent. The balloon stiffness then was a factor.

The rotometer was calibrated prior to the 25-hour performance test. The method agreed within 0.6% of a prior calibration by Fisher and Porter, using air at the same Reynolds number in the volumetric prover. The flow meter was run at a discharge pressure of 300 psia.

The use of calibrated critical orifices was attempted as a secondary measurement, but found to give serious drifting problems because of the small size required for the orifice. A well-designed, critically-operated venturi employing a 0.010-in. diameter throat was found to change performance in a matter of hours. With orifice devices, great care must be taken to keep the propellant system clean and to filter the incoming gas properly. No secondary flow measurements were taken aside from using the thrustor nozzle throat as an approximate check.

4. Power Measurements

The electric input power can be reliably measured in a Resistojet by a steady-state type voltmeter and ammeter. Unlike arc jet engines, resistance heated rockets are very steady and can be measured quite accurately by high-quality, precision D'Arsonval movements. Similarly, the meter movements are not subjected to high-frequency feedback signals potentially altering their accuracy. Because of the importance of this measurement and the ease with which it can be made, two separate sets of data were observed during the test. The maximum deviation between the two sets was 0.75% when the calibration corrections to both meter sets were applied.

The measurements of initial gas power contribution are based upon the temperature of the hydrogen at engine inlet. The resulting enthalpy values are from King, reference 26.

5. Pyrometer Measurements

An attempt was made to measure the temperature of the inner heat exchanger element by looking into the nozzle throat with an optical pyrometer. The pyrometer could not be mounted so as to provide a direct view into the nozzle, so a mirror was mounted as closely as possible to the hydrogen jet exiting the nozzle. The pyrometer was mounted outside the cell at the anti-nozzle end of the engine. The viewer sighted past the engine to the mirror which reflected the image of the nozzle.

A calibration was made by placing a lamp at the nozzle location and measuring temperature vs. lamp current. The lamp was moved outside the cell at a distance from the pyrometer equal to the sum of the previous pyrometer-to-mirror and mirror-to-nozzle distances. The temperature vs. lamp current was again measured and a window-mirror correction curve plotted. The target was taken to be a holrum with an emissivity of .95 and a correction was made for this.

Temperatures measured in this way covered a span of approximately 2100°K at the test condition. Calculated gas temperatures were above 2400°K at the same points.

There is a possibility that the nozzle throat temperature and not the inner element temperature was being measured. The small size of the nozzle places the focal point of the pyrometer in doubt. If the throat temperature were being measured, a new choice of emissivity would have to be made. This would greatly influence the corrected temperature.

APPENDIX B

Performance Definitions And Data[1]

1. Energy Efficiencies.- It is important to note that there are two efficiency definitions currently in use in electro-thermal propulsion work. Care must be exercised in making comparisons between thrustor results from different sources and particularly experimental results with theoretical analyses. A valuable criterion for defining an efficiency for any process is that it be unity when the process is perfect.

The overall total power efficiency η_o (Eq.B2) used in this report is based upon charging the thrustor with all the power supplied to it, namely propellant gas power (Eq.B3), as well as the electric (Eq.B4). The energy efficiency η_o is equivalent to that virtually always used in theoretical analysis.

$$\eta_o = \frac{\text{Effective Kinetic Power in the Jet}^{(2)}}{\text{Total Input Power}} \qquad \text{(EqB 1)}$$

$$\eta_o = \frac{F^2 (g^\circ)^2}{2 \dot{m} (P_e + P_g) \times 10^7} \qquad \text{(EqB 2)}$$

$$P_{g_i} = \dot{m}\, h_i \quad (4.187) \qquad \text{(EqB 3)}$$

$$P_e = E \quad I \qquad \text{(EqB 4)}$$

The second or overall electric power "efficiency" η_o^*, (Eq.B5) considers charging the thrustor only with the electric power supplied. Its use became established by parallelism with evaluating propulsors which accelerate the propellant strictly by electrical or magnetic forces, e.g., ionic engines, etc.

$$\eta_o^* = \frac{F^2 (g^\circ)^2}{2 \dot{m} P_e \cdot 10^7} \qquad \text{(Eq.B5)}$$

The η_o^* values can be significantly higher than η_o, for the same electro-thermal engine data, particularly at the lower specific impulse values. In fact, under cold flow conditions ($P_e = 0$), η_o^* is infinite.

(1) See page iv for units used.

(2) Actually, the energy is being evaluated through momentum consideration which is not precisely correct (ref. 27). However, since the thrust produced by a given energy expenditure is the objective, this definition is not objectionable.

As a numerical example of the two efficiencies, consider the engine data for Point 35, Run of 1 May 1965:

$$P_e = 3044 \text{ watts}$$

$$\dot{m} = 0.0793 \text{ gm/sec}$$

$$F = 65.7 \text{ gm}$$

$$T_{propellant} = 30°C$$

$$P_{propellant} = 8.79 \text{ atm.},$$

giving

$$\eta_o = 0.77 \quad \text{but} \quad \eta_o^* = 0.86$$

2. Specific Impulse.-

The observed specific impulse is defined:

$$I_{sp} = \frac{\text{measured thrust}}{\text{measured mass flow}} = \frac{F}{\dot{m}} \qquad \text{(Eq.B6)}$$

The vacuum specific impulse may be estimated if the nozzle is running "full" as:

$$I_{sp(vac)} = \frac{F}{\dot{m}} + p_{cell}\left(\frac{A_e}{\dot{m}}\right) \qquad \text{(Eq.B7)}$$

Application of this correction gives for Point 35, for illustration, an $I_{sp(vac)} = 838$ seconds. The resultant efficiency is

$$\eta_{o\,(vac)} = 0.79$$

Point No.	Thrustor Voltage volts	Current amps	Thrust grams	Mass Flow grams/sec	Test Chamber Pressure mm-Hg	Engine Chamber Pressure psia	Hydrogen Inlet Temp. °K	Outer Shell Temp., °C T_1	T_2	T_3	T_4	T_5	T_6	T_{17}	Engine Case Temp., °C T_7	T_8	T_9	T_{10}	T_{11}	T_{12}	T_{13}	T_{14}	T_{15}
1	0	0	19.8	.0748	.93	40.5	304	28	27	27	27	26	26	22	26	26	26	26	26	26	26	26	26
2	.88	37.2	20.2		---	42.0		28	28	28	28	28	28	27	28	29	29	29	29	29	29	29	29
3	1.57	80.7	22.6		---	46.2		29	28	29	28	30	29	46	44	44	44	44	43	43	43	43	46
4	2.39	115.7	26.2		---	52.8		27	27	32	27	37	32	72	66	66	66	64	61	60	59	62	68
5	3.59	139.0	30.1		---	63.3		29	31	38	28	48	39	114	106	106	102	99	92	92	91	96	107
6	4.65	152.0	35.6		---	72.0		31	32	43	28	59	47	156	151	153	149	143	131	127	124	129	143
7	5.95	159.0	38.8		---	79.9		33	34	51	28	74	56	203	203	206	201	195	177	171	168	172	189
8	7.31	161.0	42.2		.59	88.3		44	44	64	37	109	75	268	295	297	288	276	249	238	234	233	253
9	9.85	162.5	47.4		.57	97.5		50	51	76	37	139	83	357	441	443	423	403	353	328	318	316	333
10	10.93	163.0	49.7		.57	101.7		63	62	88	45	169	98	416	539	541	521	493	431	398	383	373	392
11	12.30	163.0	51.8		.58	106.4		78	72	101	52	211	116	497	676	679	656	617	536	489	471	448	471
12	13.72	[illegible]	55.4		.68	112.0		96	82	116	57	301	130	568	817	826	799	744	633	568	544	510	538
13	15.30	163.0	57.6	.0748	.61	116.0	304	142	107	146	68	322	153	683	1006	1009	966	905	773	694	664	663	652

Corrected Data From Test Run of 23 April 1965

Table XII

Point No.	Thrustor Voltage volts	Current amps	Thrust grams	Mass Flow grams/sec	Test Chamber Pressure mm-Hg	Engine Chamber Pressure psia	Hydrogen Inlet Temp. °K	Outer Shell Temp., °C T_1	T_2	T_3	T_4	T_5	T_6	Engine Case Temp., °C T_{13}	T_{14}	T_{15}	(Pyro) T_{18}
1	0	0	20.5	.0748	.95	42.0	303	27	27	27	27	27	27	27	27	27	----
2	2.4	116.0	26.1		.80	53.2	303	26	26	28	27	29	28	47	52	29	----
3	3.5	139.5	31.0		.72	63.3	304	28	28	34	26	43	37	83	93	104	----
4	5.0	152.0	36.2		.67	73.6	304	28	28	42	26	56	46	122	134	152	----
5	6.5	156.5	40.7		.63	83.5	304	33	33	54	26	81	58	188	198	217	----
6	7.4	156.0	42.5		.62	87.5	304	48	45	61	26	94	67	216	225	245	----
7	9.8	162.5	47.4		.62	99.3	304	49	46	60	43	132	77	321	317	335	----
8	12.4	163.0	51.7		.62	106.5	304	74	65	81	54	206	113	488	471	482	----
9	13.8	163.5	54.0		.65	110.8	304	99	74	98	65	260	129	587	544	566	960
10	15.1	165.5	56.6	.0748	.68	114.6	304	137	89	117	77	309	150	676	627	644	----
11	15.2	167.0	60.5	.0793	.69	121.5	304	154	102	132	80	321	160	677	633	652	1064
12	16.25	169.0	62.6		.70	123.6	304	173	111	141	84	338	164	723	667	684	1098
13	17.0	171.0	63.4		.69	126.0	303	184	123	146	96	358	178	767	709	718	1193
14	17.6	172.0	63.9		.70	127.3	303	206	128	158	96	385	181	799	739	753	1232
15	17.8	171.0	64.8		.70	128.7	303	215	133	167	100	398	186	811	754	769	1248
16	17.7	171.0	64.8		.70	129.4	304	221	139	172	102	405	189	817	762	776	----
17	17.8	171.0	64.8		.70	129.1	303	231	147	212	76	414	193	823	778	784	----
18	17.8	171.0	64.9		.70	128.7	304	234	157	214	84	412	203	822	776	784	----
19	17.8	171.0	65.1		.70	129.1	304	251	151	207	81	412	200	827	792	788	----
20	17.8	171.0	65.0		.69	129.1	304	241	154	211	84	417	201	836	789	797	----
21	17.8	171.0	64.9		.68	128.7	304	225	145	209	75	408	192	818	764	777	----
22	17.8	171.0	65.1		.68	128.7	304	222	151	206	81	405	198	814	769	777	----
23	17.8	171.0	65.1		.69	128.7	304	233	151	206	81	407	197	816	771	778	1260
24	17.8	171.0	65.1		.69	128.7	304	233	151	206	83	411	197	828	775	787	----
25	17.8	171.0	65.3		.70	129.1	304	233	151	206	82	409	196	820	775	781	----
26	17.8	171.0	65.3		.70	129.1	304	233	151	206	81	408	197	817	773	780	----
27	17.8	171.0	65.5		.70	129.1	304	231	151	204	80	407	196	820	767	778	----
28	17.8	171.0	65.6		.70	129.1	304	226	145	208	78	417	200	828	773	783	1254
29	17.8	171.0	65.3		.70	129.1	304	233	151	206	83	413	198	828	775	781	----
30	17.8	171.0	65.7		.70	129.1	304	234	153	207	83	414	199	824	778	783	----
31	17.8	171.0	65.7		.70	129.1	304	232	151	206	82	413	199	827	773	777	----
32	17.8	171.0	65.8		.70	129.1	303	232	152	207	83	416	199	830	777	782	----
33	17.8	171.0	65.7		.70	129.1	304	232	153	207	82	413	199	821	777	779	----
34	17.8	171.0	65.7	.0793	.70	129.1	303	231	151	205	82	413	197	819	774	777	----

CORRECTED DATA FROM TEST RUN OF 30 APRIL 1965

Table X[illegible]

Point No.	Thrustor Voltage volts	Current amps	Thrust grams	Mass Flow grams/sec	Test Chamber Pressure mm-Hg	Engine Chamber Pressure psia	Hydrogen Inlet Temp. °K	Outer Shell Temp., °C T_1	T_2	T_3	T_4	T_5	T_6	Engine Case Temp., °C T_{13}	T_{14}	T_{15}	(Pyro) T_{18}
35	17.8	171.0	65.7	.0793	.70	129.1	303	237	148	204	82	414	193	824	771	782	----
36	17.8	171.0	65.7		.70	129.1	303	233	150	177	113	418	193	832	779	785	----
37	17.8	171.0	65.8		.70	129.1	303	232	151	177	113	416	199	821	774	788	----
38	17.8	171.0	65.8		.70	129.1	303	232	152	177	112	416	199	821	778	779	----
39	17.8	171.0	65.8		.70	129.1	303	219	149	176	113	416	199	827	774	777	----
40	17.8	171.0	65.8		.70	129.1	303	232	150	188	102	416	199	826	772	777	----
41	17.8	171.0	66.3		.70	131.0	303	220	149	174	111	416	198	819	776	777	----
42	17.8	170.5	65.7		.70	129.1	303	220	149	174	114	418	199	817	777	783	----
43	17.8	171.0	65.7		.70	129.1	303	223	145	178	107	420	193	826	773	780	----
44	17.8	171.0	65.8		.69	129.1	303	219	151	173	116	418	197	828	774	778	----
45	17.8	171.0	65.8		.69	129.1	304	233	161	201	101	422	203	827	773	781	----
46	17.8	171.0	65.8		.68	130.0	304	233	151	189	101	417	197	826	772	789	----
47	17.8	171.0	65.7		.68	130.0	304	220	151	198	89	421	193	826	773	789	1258
48	17.8	170.0	65.0		.68	129.1	304	228	151	203	86	414	198	822	769	773	----
49	17.8	170.5	65.3		.68	129.1	304	228	147	200	86	414	197	817	773	776	----
50	14.1	187.0	63.3		.68	125.7	304	213	147	192	92	410	197	787	751	759	----
51	15.3	198.0	64.5		.69	127.8	304	206	142	188	81	378	186	782	725	724	----
52	15.45	196.5	64.7		.69	129.1	304	217	140	197	84	418	191	819	769	777	----
53	15.4	197.5	65.8		.69	130.5	304	213	145	195	89	384	197	813	762	772	----
54	15.4	197.5	65.8		.69	130.5	304	215	147	197	90	413	198	817	766	775	----
55	15.4	197.5	65.4		.69	130.5	304	214	148	197	84	417	192	816	764	773	----
56	15.4	197.5	64.7		.69	129.1	304	217	142	198	84	416	192	815	763	772	----
57	15.4	198.0	65.1		.69	130.0	304	224	151	197	90	414	197	814	769	775	----
58	15.4	198.0	65.6		.69	130.0	304	213	148	196	89	414	197	819	768	776	----
59	15.3	197.5	64.9		.68	130.0	304	212	148	195	89	411	197	813	762	770	----
60	15.3	198.0	65.0		.68	130.0	304	211	146	194	89	409	196	806	762	766	----
61	15.25	198.7	65.3		.68	130.0	304	213	139	196	84	411	191	806	753	762	----
62	15.25	198.7	65.2		.67	129.6	304	219	147	194	89	412	196	814	763	772	----
63	15.25	199.0	65.6		.67	130.4	304	209	146	193	89	407	194	806	756	764	----
64	15.2	199.5	64.5		.67	129.1	304	208	146	194	89	406	194	797	756	761	----
65	12.7	183.0	61.1		.67	121.0	304	203	144	186	93	399	193	773	736	747	----
66	9.55	179.0	55.7		.67	110.0	303	155	133	166	78	294	173	524	528	553	----
67	5.4	166.0	45.5		.70	87.9	303	108	102	122	56	159	122	253	270	289	----
68	0	0	21.5	.0793	.90	44.4	303	36	37	37	33	32	32	31	31	31	----
69	0	0	20.8	.0748	.90	43.0	303	36	37	37	33	32	32	31	31	31	----

CORRECTED DATA FROM TEST RUN OF 30 APRIL 1965

Table XIII (cont'd)

REPORT DISTRIBUTION LIST FOR
CONTRACT NASW-1070

NASA-Lewis Research Center (1)
Spacecraft Technology Division (MS54-5)
21000 Brookpark Road
Cleveland, Ohio 44135
Attn: J. H. Childs

NASA Headquarters (2)
FOB-10B
600 Independence Avenue, N.W.
Washington, D.C. 20546
Attention: RNT/J. Lazar
/J. Mullen

NASA-Lewis Research Center (1)
Spacecraft Technology Procurement Section
21000 Brookpark Road
Cleveland, Ohio 44135
Attn: J. H. DeFord

NASA-Lewis Research Center (4)
Electrothermal Technology Section (MS54-5)
21000 Brookpark Road
Cleveland, Ohio 44135
Attn: H. R. Hunczak

NASA-Lewis Research Center (1)
21000 Brookpark Road
Cleveland, Ohio 44135
Attn: Reports Control Office

NASA-Lewis Research Center (1)
21000 Brookpark Road
Cleveland, Ohio 44135
Attn: Technical Information Division

NASA-Lewis Research Center (1)
Technology Utilization Office
21000 Brookpark Road
Cleveland, Ohio 44135

NASA-Lewis Research Center (1)
Library
21000 Brookpark Road
Cleveland, Ohio 44135

NASA Scientific and Technical (6)
Information Facility
Box 5700
Bethesda, Maryland 20014
Attn: NASA Representative RQT-2448

NASA Marshall Space Flight Center (1)
Library
Huntsville, Alabama 35812

NASA Marshall Space Flight Center (1)
R-RP-DIR
Bldg. 4481
Huntsville, Alabama 35812
Attn: G. Heller

NASA Ames Research Center (1)
Library
Moffett Field, California 94035

NASA Langley Research Center (1)
Library
Hampton, Virginia 23365

NASA Goddard Space Flight Center (1)
Library
Greenbelt, Maryland 20771

NASA Goddard Space Flight Center (1)
Bldg. 6
Greenbelt, Maryland 20771
Attn: W. Isley, Code 623

Commander (1)
Aeronautical Systems Division
Wright-Patterson AFB, Ohio 45433
Attn: AFAPL (APIE), P. Lindquist

AFWL (1)
Kirtland AFB, New Mexico
Attn: WLPC/Capt. C. F. Ellis

AVCO Corporation (1)
Research and Advanced Development Division
201 Lowell Street
Wilmington, Massachusetts
Attn: Dr. R. John

Electro-Optical Systems, Inc. (1)
125 N. Vinedo Avenue
Pasadena, California
Attn: Dr. R. Buhler

General Electric Company (1)
Electric Space Propulsion Projects
Evandale, Ohio
Attention: Dr. M. L. Bromberg

Gianinni Scientific Corporation (1)
3839 South Main Street
Santa Ana, California
Attn: Adriano Ducati

Aerospace Corporation (1)
P. O. Box 95085
Los Angeles 45, California
Attn: Library Technical Documents Group

Ling-Temco-Vought, Inc. (1)
Advanced Systems, Astro, Division
Box 6267
Dallas 22, Texas
Attn: F. T. Esenwein

Westinghouse Astronuclear Laboratories (1)
Electrical Propulsion Laboratory
Pittsburgh 34, Pennsylvania
Attn: H. W. Szymanowski, Manager

Grumman Aircraft Eng. Co. (1)
Thermodynamics and Propulsion Section
Plant #5
Bethpage, N. Y.
Attn: I. Tobias

Jet Propulsion Laboratory (1)
California Institute of Technology
4800 Oak Grove Drive
Pasadena, California
Attn: John W. Stearns, Jr. MS 125-224

National Security Agency A44 (1)
Fort George G. Mead, Maryland
Attn: Lt. John D. Ryder, Code 188-7250

THE DESIGN AND PERFORMANCE OF A 3 KW CONCENTRIC TUBE RESISTOJET

by

R. J. Page and R. A. Short

ABSTRACT

34239

A 3 kw concentric tube resistojet, using hydrogen as a propellant, was designed for operation from solar cell power supplies. A heat exchanger of unique geometry made possible by the tungsten vapor-deposition process permitted cool operation and hence longer life for the boron nitride insulators. In a 25-hour performance test in a vacuum, a specific impulse of 828 seconds was measured at an overall total power efficiency of 0.77, using a precision thrust dynamometer. Stagnation chamber conditions of 8.8 atmospheres and 2417°K were measured. High life-expectancy and reliability are apparent features of the design. Author